Stiffness of the Proximal Tibial Bone in Normal and Osteoarthritic Conditions: A Parametric Finite Element Simulation Study

A Thesis Submitted to the College of

Graduate Studies and Research

in Partial Fulfillment of the Requirements

for the Degree of Master of Science

in the Department of Mechanical Engineering

University of Saskatchewan

Saskatoon

By

Morteza Amini

PERMISSION TO USE

In presenting this thesis/dissertation in partial fulfillment of the requirements for a Postgraduate degree from the University of Saskatchewan, I agree that the Libraries of this University may make it freely available for inspection. I further agree that permission for copying of this thesis/dissertation in any manner, in whole or in part, for scholarly purposes may be granted by the professor or professors who supervised my thesis/dissertation work or, in their absence, by the Head of the Department or the Dean of the College in which my thesis work was done. It is understood that any copying or publication or use of this thesis/dissertation or parts thereof for financial gain shall not be allowed without my written permission. It is also understood that due recognition shall be given to me and to the University of Saskatchewan in any scholarly use which may be made of any material in my thesis/dissertation.

DISCLAIMER

Reference in this thesis/dissertation to any specific commercial products, process, or service by trade name, trademark, manufacturer, or otherwise, does not constitute or imply its endorsement, recommendation, or favoring by the University of Saskatchewan. The views and opinions of the author expressed herein do not state or reflect those of the University of Saskatchewan, and shall not be used for advertising or product endorsement purposes.

Requests for permission to copy or to make other uses of materials in this thesis/dissertation in whole or part should be addressed to:

Head of the Department of Mechanical Engineering
University of Saskatchewan
Saskatoon, Saskatchewan S7N 5A9
Canada

OR

Dean
College of Graduate Studies and Research
University of Saskatchewan
107 Administration Place
Saskatoon, Saskatchewan S7N 5A2
Canada

Abstract

Background: Osteoarthritis (OA) is a debilitating joint disease marked by cartilage and bone changes. Morphological and mechanical changes to bone, which are thought to increase overall bone stiffness, result in distorted joint mechanics and accelerated cartilage degeneration. Using a parametric finite element (FE) model of the proximal tibia, the primary objective of this study was to determine the relative and combined effects of OA-related osteophyte formation, and morphological and mechanical alterations to subchondral and epiphyseal bone on overall bone stiffness. The secondary objective was to assess how simulated bone changes affect load transmission in the OA joint.

Methods: The overall geometry of the model was based on a segmented CT image of a cadaveric proximal tibia used to develop a 2D, symmetric, plane-strain, FE model. Simulated bone changes included osteophyte formation and varied thickness and stiffness (elastic modulus) in subchondral and epiphyseal bone layers. Normal and OA related values for these bone properties were based on the literature. "Effective Stiffness (K)" was defined as the overall stiffness of the proximal tibia, calculated using nodal displacement of the loaded area on the subchondral cortical bone surface and the load magnitude.

Findings: Osteophyte formation and thickness or stiffness of the subchondral bone had little effect on overall bone stiffness. Epiphyseal bone stiffness had the most marked effect on overall bone stiffness. Load transmission did not differ between OA and normal bone.

Interpretation: Results suggest that epiphyseal (trabecular) bone is a key site of interest in future analyses of OA and normal bone. Results also suggest that observed OA-related alterations in epiphyseal bone may result in OA bone being more flexible than normal bone.

Preface

Sections of this thesis have been submitted as a multi-authored paper in a refereed journal. The research, data analyses and manuscript preparation were carried out by me and the co-authors contributed in editing the manuscripts for submission to refereed journals.

Submitted Paper

Amini M, Szyszkowski W, Lanovaz JL, Kontulainen S, Johnston JD. *Stiffness of the proximal tibial bone in normal and osteoarthritic conditions: a parametric finite element simulation study*. Journal of Biomechanics. Submitted on November 28th 2012.

Author's contribution: Morteza Amini was jointly responsible for the original ideas behind the paper, developing the model, image and mechanical data analyses, presentation of the findings, and writing and editing of the original paper. Dr. Walerian Szyszkowski was jointly responsible for the original ideas, provided supervision, and edited the paper. Dr. Joel Lanovaz was jointly involved in interpretation of study findings and editing of the paper. Dr. Saija Kontulainen edited the paper. Dr. JD Johnston was jointly responsible for the original ideas, provided supervision, and was the key editor of this paper.

The results in this study were presented at local and national conferences:

i. Amini, M., J.L. Lanovaz, W. Szyszkowski, J.D. Johnston, Mechanics of proximal tibial bone in osteoarthritis conditions: A parametric simulation study, Oral presentation in Canadian Society of Biomechanics (CSB) biannual conference, Vancouver, BC, June 2012.

ii. Amini, M., J.L. Lanovaz, W. Szyszkowski, J.D. Johnston, Mechanics of proximal tibial bone in osteoarthritis conditions: A parametric simulation study, Presented in 19th Life & Health Science Research Day, Saskatoon, SK, March 2012.

Acknowledgement

First and foremost I would like to thank my supervisors, Dr. JD Johnston and Dr. Walerian Szyszkowski, for all their support. My special thanks go to Dr. JD Johnston whose guidance and help I am truly grateful of and without his support this thesis would not have been possible. He was the one who was patient while I was learning how to conduct a research and supported me at every step of my work. I thank Dr. Walerian Szyszkowski for his supervision, invaluable advice and his generosity in teaching new material at any chance during my MSc.

My sincerest thanks go to my dearest Mom, Dad, my brother Reza and my sister Fereshteh for their heartwarming love and encouragement throughout all of my university studies. Especially the constant support of my only family members in Canada, Fereshteh, has kept me going through all ups and downs of my life far from home.

Many thanks to S. Majid Nazemi for his insightful discussions and comments about my work and for being there for me when I needed help.

My appreciation goes to my friends at the MOBILab, for their support and for making my time here more enjoyable.

Table of Contents

List of Tables

List of Figures

List of Abbreviations, Symbols and terms

Terms	Definition
Axial	Plane that divides the body into superior and inferior parts; synonymous with transverse plane
Cancellous	Type of bone tissue comprised of vertical and horizontal trabeculae which create a spongy, cellular-like tissue; typically occurs at the ends of long bones; high surface area compared to cortical bone and is therefore more metabolically active; synonymous with trabecular bone
Cortical bone	Type of bone tissue comprised of multiple layers of compacted bone; forms the cortex or outer shell of bone; much denser, stronger and stiffer than cancellous bone; synonymous with compact bone
Distal	Pertains to different ends of an extremity; distal end of extremity is the end situated farthest from the center of the body (e.g., distal tibia is located at ankle joint)
Lateral	Situated at or extending to the side
Material stiffness	Describes intrinsic material properties of bone itself; independent of specimen geometry or size; synonymous with mechanical stiffness
Mechanical stiffness	Describes intrinsic material properties of bone itself; independent of specimen geometry or size; synonymous with material stiffness
Medial	Situated at or extending to the middle
Osteophyte	Bony projection that forms along the periphery of joints, also known as bone spurs
Proximal	Pertains to different ends of an extremity; proximal end of extremity is the end situated nearest the center of the body (e.g., proximal tibia is located at knee joint)
Sclerosis	Generally referred to as a stiffening or hardening of a structure
Structural stiffness	Describes bone's response to deflection; dependent upon both mechanical stiffness properties and physical size of the bone tissue being tested
Subchondral bone	Bone below (sub) cartilage (chondral)
Trabecular bone	Type of bone tissue comprised of vertical and horizontal trabeculae which create a spongy, cellular-like tissue; typically occurs at the ends of long bones; high surface area compared to cortical bone and

	is therefore more metabolically active; synonymous with cancellous bone
Trabeculae	Latin for “small beam”; bone tissue element in the form a small beam, strut or rod

Abbreviation	Definition
2D	Two dimensional
3D	Three dimensional
CT	Computed tomography
DEXA	Dual energy x-ray absorptiometry, same as DXA
FE	Finite element
MRI	Magnetic resonance imaging
OA	Osteoarthritis
QCT	Quantitative computed tomography
SCT	Subchondral cortical thickness
SCS	Subchondral trabecular stiffness (elastic modulus)
STT	Subchondral trabecular thickness
STS	Subchondral trabecular stiffness (elastic modulus)
ETS	Epiphyseal trabecular stiffness (elastic modulus)
MTS	Metaphyseal trabecular stiffness (elastic modulus)
OD	Osteophyte Diameter

Symbol	Definition
σ	Stress (Pa)
ε	Strain
ρ	Density (kg/m^3)
υ	Poisson's ratio
δ	Deflection (mm)
E	Material stiffness, Modulus of elasticity, Young's modulus (MPa)
F	Force (N)

1 Introduction

1.1 Overview

Knee osteoarthritis (OA) is a debilitating joint disease marked by cartilage degeneration and underlying bone changes in form of osteophyte formation along peripheral edges of the bone and morphological and mechanical changes in subchondral and epiphyseal regions [1, 2]. OA causes pain and limited motion in the affected joint and, as the most common joint disease, has affected over 3 million Canadians [3]. Due to limited knowledge about OA pathogenesis (i.e. how OA is initiated and progressed), there is still no cure for this disease.

It has been reported that with OA, bony regions near the cartilage surface (subchondral cortical and trabecular bone) have shown higher thickness and density [4-10]. One predominant theory proposes that higher stiffness and amounts of subchondral bone will result in an overall stiffer bone under the cartilage layer, which will alter the load and stress distribution in cartilage, leading to cartilage degeneration and eventual OA [8, 11]. Specifically, a stiffened bone will be less able to deform under dynamic impact loading (resulting in higher average dynamic stresses), and leading to concentrations of the energy being transferred through particular sections of the cartilage, and generating higher internal cartilage stresses [8, 10-13]. Conversely, with OA it has also been reported that bony regions distal to the subchondral bone surface (epiphyseal trabecular bone) have shown lower quantities of bone [5, 14-19] which may decrease, not increase, the overall structure stiffness of bone. Though unproven, it has been speculated that subchondral bone changes offset reductions at epiphyseal trabecular bone sites, leading to a stiffer overall structure [8, 11]. To improve our understanding of the mechanical role of bone in OA, we need to evaluate how alterations in subchondral and epiphyseal bone thickness and

stiffness associated with OA affect the overall stiffness of bone directly at the subchondral bone surface, which is most relevant for overlying cartilage integrity and health.

Structural, morphological and mechanical alterations in subchondral and epiphyseal bone will affect how load is transmitted from the subchondral bone surface to the diaphysis. In the normal bone, load is transmitted through subchondral cortical bone through trabecular regions to the metaphysis and cortical diaphysis. Load is also transmitted along the peripheral cortices to the cortical diaphysis. With OA, it has been proposed that decreased quantities of bone at distal epiphyseal sites are due to 'stress shielding', whereby the majority of load is transmitted along the periphery—perhaps due to osteophyte formation [20, 21]—leading to less load applied in trabecular regions and subsequent trabecular bone resorption. However, it is currently unknown how OA-related osteophyte formation and morphological and mechanical alterations in subchondral and epiphyseal bone affect load transmission in the OA joint.

A parametric finite element (FE) modeling technique can be applied to investigate the effects of different mechanical and morphological alterations on overall structural stiffness and load transmission, while also considering the degree of geometrical complexity of bone structure at the proximal tibia. Parametric FE analysis provides a non-invasive, time and cost efficient method to study complicated structures such as human knee, and can be used to directly evaluate the effect of individual morphological and mechanical property changes on overall bone stiffness and load transmission. To date, few studies have focused on OA bone stiffness and load transmission using FE method [22-24]. Stress elevation in the cartilage layer after artificial stiffening of subchondral cortical bone has been documented using a simplified model of the bone [25]. To date, there have been no studies evaluating the effects of individual and combined

alterations in morphological and mechanical properties of subchondral and epiphyseal bone on overall bone stiffness.

Using a parametric FE model of the proximal tibia, the primary objective of this study was to determine individual and combined effects of OA-related osteophyte formation and morphological and mechanical changes to subchondral and epiphyseal bone on overall bone stiffness. The secondary objective was to determine how OA-related bone alterations affect load transmission in the OA joint.

1.2 Scope

Chapter 2 is a literature review on the anatomy of the knee joint and the etiopathogenesis of the osteoarthritis disease, outlining the mechanical alterations involved in OA disease initiation and progression. Chapter 2 also introduces Finite Element modeling technique as a tool to assess OA subchondral bone with a brief technical background. Chapter 3 includes the research questions and study objectives. Chapter 4 outlines the methodological details of our parametric FE analysis of the OA proximal tibia. Chapter 5 describes the individual and combined effects of the parameters on the overall subchondral bone stiffness as results of our FE analysis. Chapter 6 discusses our findings in comparison with the existing body of literature, and outlines the main strengths and limitations of this study. Chapter 7 outlines conclusions and significances related to our study, and offers recommendations for future research.

2 Literature Review

2.1 Functional Anatomy

2.1.1 Knee Joint

The knee joint consists of three bones; the proximal tibia, the distal femur and the patella (Fig 2-1). The patella is articulated with the distal femur through patello-femural joint and the tibio-femural articulating joint links distal femur to proximal tibia. The proximal tibia, which is the most commonly affected OA site, is subject of our study. There are two load bearing compartments in proximal tibia; the medial and lateral compartments (Fig 2-1). The medial compartment compared to the lateral, bears more load during stance phase of gate [26].

2.1.2 Articular Cartilage and Meniscus

The joint surfaces of all three bones forming the knee joint are covered by a thin layer of resilient tissue called articular cartilage. This relatively soft layer is comprised of a low friction bearing material which also transmits loads between bones (Fig 2-1 & 2-2). The highly hydrated proteoglycan matrix and type II collagen fibers provide stiffness and deformation resistance under compressive and tensile loadings for the cartilage layer. Accordingly, cartilage can be considered as a poroviscoelastic fibril reinforced composite structure with around 75% water content [27]. Cartilage also has an avascular structure with limited repair and regeneration capacity.

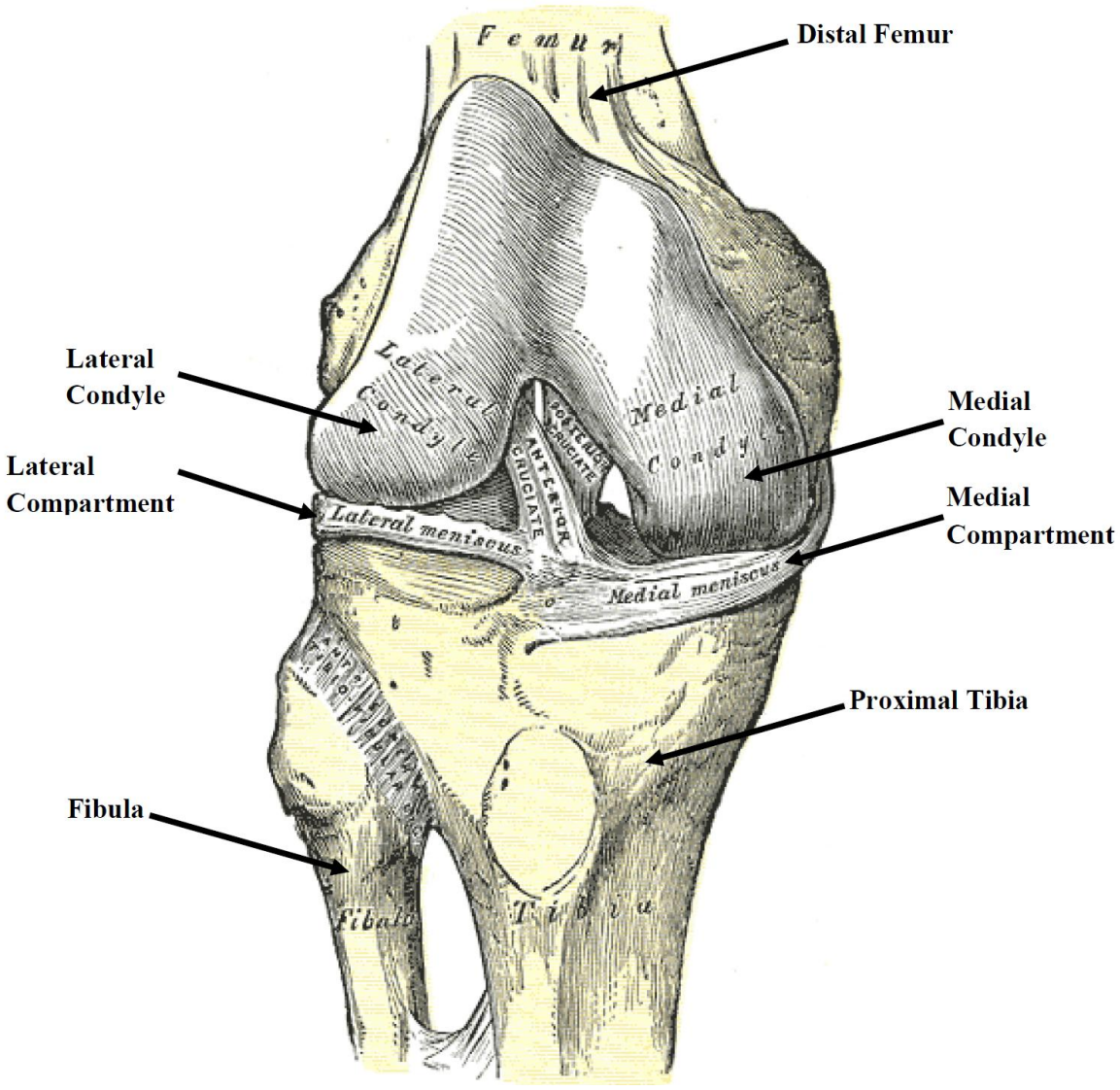

Figure 2-1) Anterior view of the knee joint and the constituent bones. Displayed bones include the proximal tibia and corresponding medial and lateral compartments, fibula, and the distal femur and corresponding medial and lateral condyles. Modified from Gray's Anatomy [28].

The meniscus is comprised of two C-shaped fibrocartilage wedges lying between the articular surfaces of the distal femur and proximal tibia, which are attached to the medial and lateral proximal tibial compartments (Fig 2-2). The main functions of the menisci are stability of the joint and the load transmission between two articular cartilage surfaces during loading and movements [29-31].

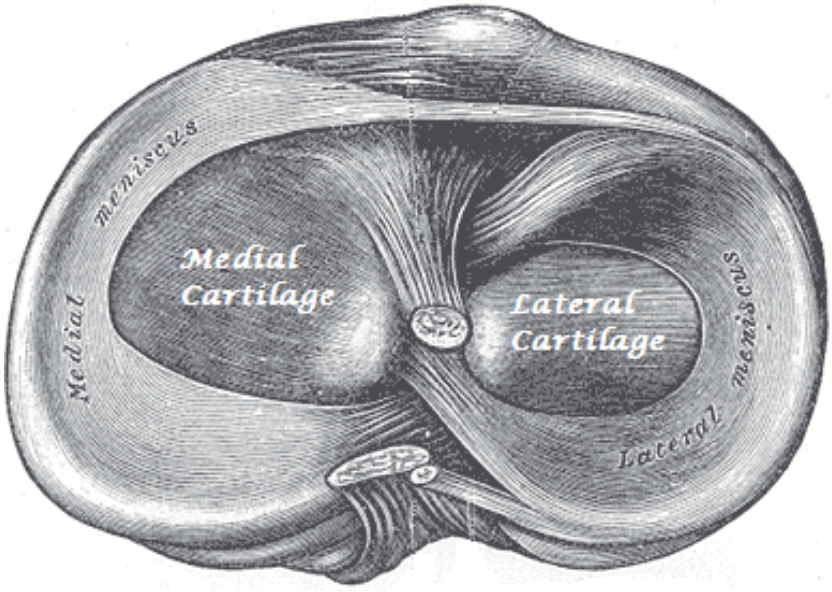

Figure 2-2) Axial view of the structure of the proximal tibial articulating surface, including medial and lateral menisci which overlie the medial and lateral articular cartilage. The Menisci and cartilage layers serve as low friction bearing material as well as transmitting load between the distal femur and proximal tibia. Modified from Gray's Anatomy [28].

2.1.3 Subchondral bone

Various bony layers lie right beneath the articular cartilage layer with the following order:

- Subchondral cortical bone (also called subchondral plate or endplate), a very thin but compact bony layer (Fig 2-3 & 2-4)
- Subchondral trabecular bone, with a porous cancellous structure supporting the overlying subchondral cortical bone. The structural elements of trabecular bone are rod/plate like elements called trabeculae (Figure 2-3 & 2-4)
- Epiphyseal trabecular bone fills the proximal epiphysis of the bone (Figure 2-4)
- Metaphyseal trabecular bone fills the proximal metaphysis of the bone and usually is less compact compared to subchondral/epiphyseal trabecular bone (Figure 2-4)

"Subchondral bone" term refers to the overall subchondral bone structure which supports the joint and also plays the main role in load transmission between the articulating bones [32].

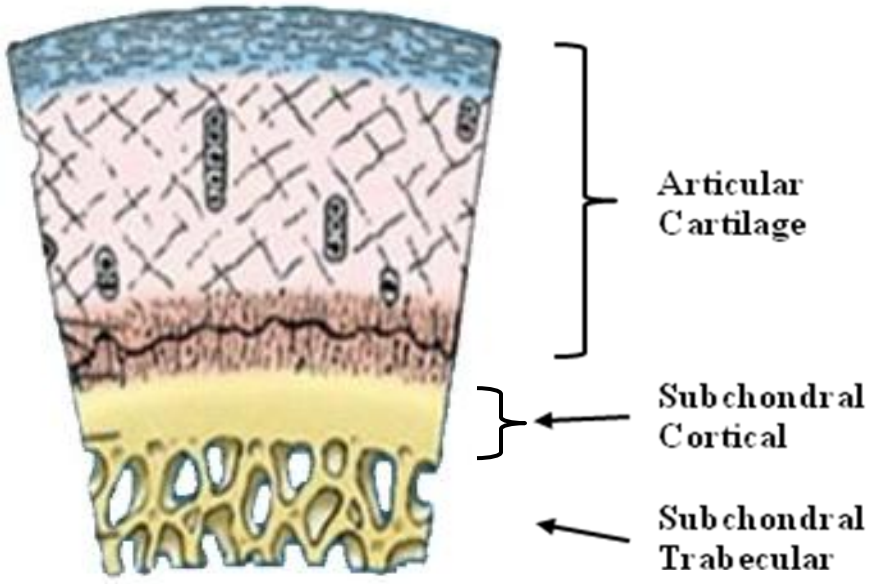

Figure 2-3) Schematic drawing of the different layers of the cartilage-subchondral bone complex, including articular cartilage, subchondral cortical and subchondral trabecular bone. Modified from Geistlich Surgery [33].

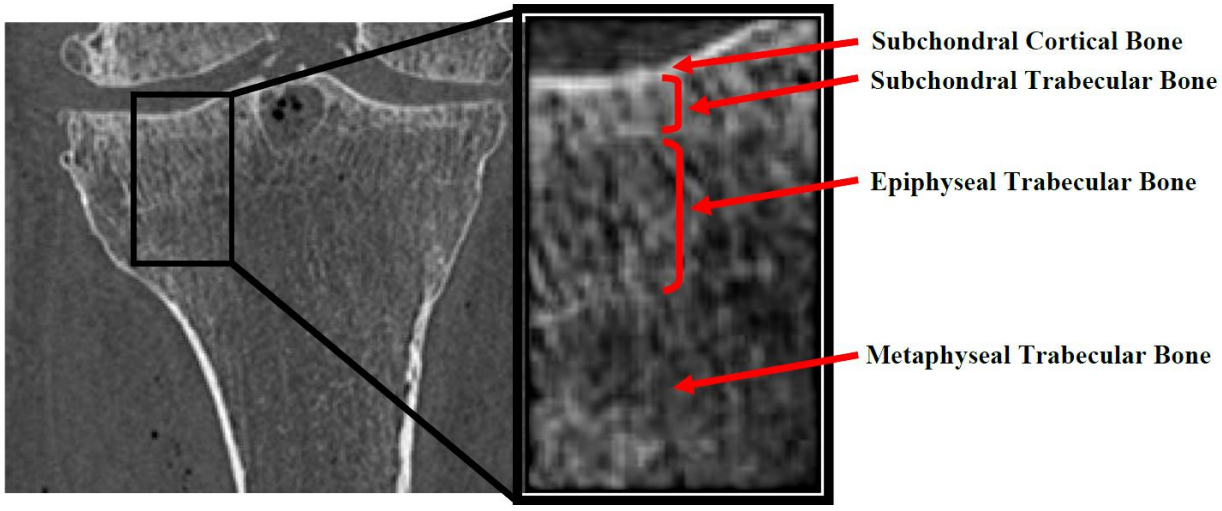

Figure 2-4) Mid-coronal computed tomography (CT) image of the proximal tibia and pertinent bony components, including subchondral cortical, subchondral trabecular, epiphyseal trabecular and metaphyseal trabecular bone. Neither cartilage nor the meniscus is observable in this image because neither tissue can absorb radiation.

2.2 Osteoarthritis

2.2.1 Disease characteristics

OA is characterized by clinical symptoms such as joint pain, swelling, stiffness and limited range of motion in the affected joint; morphological alterations including loss of cartilage in load bearing sites and subchondral bone sclerosis (bone hardening); and also biomechanical alterations, including altered mechanical properties of OA cartilage (decreased tensile, shear and compression stiffness) [34, 35] and bone (stiffness) [1]. Regarding OA subchondral bone, it was long thought to be stiffer than normal [36, 37], but recent studies at knee and hip have shown OA bone to be less stiff than normal bone [38-43]. This contradiction in results may be due to the fact that most of these studies have focused on an isolated tissue from a specific layer; however, each layer of subchondral bone may be affected differently and experience various mechanical alterations during stages of OA disease progression.

2.2.2 Etiopathogenesis

Traditionally, OA is recognized by its effects on the cartilage layer and is generally assumed to be a disease of cartilage [4]. However, significant alterations in the subchondral bone morphology and mechanical properties have been reported in association with OA initiation and progression. Although the exact initiation and progression mechanism of OA is still unclear, previous studies suggest two major cause theories: first, OA is considered to be a disease targeting articular cartilage, and the damaged cartilage causes changes in underlying bone. Based on this theory—which is most commonly analyzed by OA researchers—impact loading, fatigue loading or changes in joint mechanics will damage the cartilage structure and finally lead to cartilage breakdown and OA [44].

The second theory, which has recently gained increased attention, has focused on the OA subchondral bone mechanical and morphological properties in OA initiation and progression. According to this theory, altered subchondral bone stiffness and thickness alter the supporting function of subchondral bone, which causes changes in stresses within overlaying cartilage [10]. One hypothesis regarding the second theory is that OA subchondral bone is stiffer than normal, with decreased ability to deform under dynamic impact loading (resulting in higher average dynamic stresses), leading to concentrations of the energy being transferred through particular sections of the cartilage, and generating higher internal cartilage stresses [8, 10-13]. Higher stresses in cartilage layer will damage this layer and lead to OA [10].

Other studies have shown decreased density at the epiphyseal trabecular regions (or so called subarticular trabecular bone) deep to thickened (and sclerotic) subchondral cortical bone in OA tibial samples [17, 45-47]. Researchers [47] have suggested that there might be a link between the observed local osteoporosis under the sclerotic subchondral cortical and trabecular bone and the "stress shielding" theory. Based on this theory, the altered structure and mechanical properties of the subchondral cortical and subchondral trabecular bone might result in altered load transmission pattern, and decrease loading on the epiphyseal trabecular bone, leading to bone remodeling and bone resorption (i.e., bone absorption) [47]. However, this hypothesis has not yet been tested using structural analyses of the bone structure. Another proof of stress shielding theory is proposed to be the local osteoporotic trabecular bone adjacent to the peripheral osteophytes in OA bones [21, 47]. Osteophyte formation is considered to be one of the main radiographic features of OA [20, 21], appearing at the peripheral edge of the articular surface in form of bone outgrowth [20]. This abnormal bony feature is suggested to have stress shielding effect on the bone adjacent to the osteophyte formation site, resulting in thinner

trabeculae at this region [20]; implying that the presence of osteophytes would alter the load transmission pattern inside the bone. In the normal bone, load is primarily transmitted through subchondral cortical bone through trabecular regions to the metaphysic and cortical diaphysis. In the osteophytic OA bone, load would be transmitted through cortical bone and peripheral osteophytes to the cortical diaphysis, thereby diverting load from trabecular bone, resulting in "stress shielding" and localized bone loss (due to bone remodeling). However, there is a lack of studies to determine the structural role of the osteophyte formation and its hypothesized effect on the load transmission mechanism within the bone.

2.3 Osteoarthritic Subchondral Bone

2.3.1 Qualitative Analysis

The morphologic and mechanical alterations in the bone are usually investigated using measures which assess the material density of the bone tissue and the amount of bone within a fixed volume. These measures include bone material density (bone mass / bone volume) and bone volume fraction (bone volume / total specimen volume). The product of bone volume fraction and bone material density results in definition of bone mineral density (BMD), also known as apparent BMD. These measures are generally used as surrogate estimates of bone stiffness in a sense that more quantity of bone would result in a stiffer bone. Mechanical properties of bone, at the material level, are typically reported using material stiffness (slope of the stress-strain curve, called "Young's modulus of elasticity", E). At the structural level, structural stiffness (slope of the load-displacement curve, N/mm) is used to indicate how a bone specimen comprised of different tissues responds to loading. Structural stiffness is dependent on bone specimen's geometry and mechanical properties of tissues comprising the structure.

OA has been shown to affect both morphological and mechanical properties of bone. The extent to which these alterations may occur in the subchondral bone has been shown to be in correlation with the stage of OA disease and the depth from the subchondral bone surface, and each layer of the subchondral bone (subchondral cortical, subchondral trabecular and epiphyseal trabecular bone) is affected differently during OA progression [38, 40, 42, 43, 48-50].

2.3.2 Morphology

The subchondral cortical thickness in normal and OA samples varies from 0.02 to 4.8 mm in different regions, with higher thicknesses observed at the central regions of the medial and lateral compartments, where higher loading occurs, and the lower thicknesses observed at the peripheral edges of the bone [23, 47, 51-53]. Higher subchondral cortical bone thicknesses have been reported in OA joints compared with normal samples [36, 46, 47]. A study has reported OA subchondral cortical bone thicknesses up to 2 times of normal samples [47].

2.3.3 Bone Volume

In the subchondral trabecular region, three morphological parameters are affected by OA: trabecular thickness (thickness of each trabecula); trabecular spacing (the space between the trabeculae); and bone volume fraction. Generally, in regions closer to the OA subchondral bone surface, a significant increase in bone volume fraction (the combination of subchondral cortical bone thickness and quantity of trabecular bone) and trabecular thickness have been observed [4, 49, 54-56]. A 19-70% increase with early OA and 29-93% increase with late OA in bone volume fraction have been reported [4, 54]. The high bone volume fraction in OA subjects have been suggested to be mainly due to increased thickness of the trabeculae [4, 54].

2.3.4 Material Density

Besides morphological alterations in different layers of subchondral bone, OA related bone material density alterations have also been reported. The material density (bone mass / bone volume) of the subchondral cortical, subchondral trabecular and epiphyseal trabecular bone has been reported to be lower in OA subjects [37, 46, 49, 57]. This is due to the higher bone turnover rate in these regions resulting in hypomineralized (insufficiently mineralized) bone with less material density [58].

2.3.5 Apparent Density

Volumetric apparent density of bone (bone mass / total volume) is a laboratory based measure which is the product of material density and bone volume fraction. Significant increases of volumetric apparent density in both OA knee (~50%) and OA hip (~20%) have been reported [37, 38, 40, 59]. As higher values of this measure would due to either higher material density or bone volume fraction, it can be concluded that higher bone volume fraction observed with OA offsets the relative decrease in bone material density, resulting in higher observed volumetric apparent density.

2.3.6 Mechanical Properties

The subchondral bone surface is the conjunction between the cartilage layer and the proximal tibial bone. Therefore the overall structural stiffness of the bone on this surface is the reflection of bone's response to loading on the cartilage layer. There is a lack of studies focusing on the structural stiffness of the bone directly at the subchondral cortical surface. Due to the complex surface geometry of the bone and the low thicknesses of the subchondral cortical and subchondral trabecular layers (<5mm) [13], many assessment tools are not well-suited to separately study these layers. Most studies targeting the OA and normal proximal tibia have

studied the stiffness of the epiphyseal trabecular and metaphyseal trabecular bone, while only a few have assessed the subchondral cortical bone in isolation [38, 39, 43].

The main studies comparing OA and normal bone material properties have used samples from the hip [36, 37]. These studies reported morphologic differences including higher subchondral cortical bone thickness, and higher bone volume fraction and BMD in OA bones. These studies also reported lower subchondral cortical and subchondral trabecular material stiffness. However, the authors suggested that, due to higher amount of bone in the subchondral trabecular region, the OA subchondral trabecular bone was stiffer than normal [37]. They also suggested that with higher amount of bone in the subchondral cortical bone (thicker than normal subchondral bone), this would overcome the effects of lower material stiffness in this layer. They hypothesized that the combined effect of OA related alterations in subchondral cortical and subchondral trabecular bone would result in an overall higher *structural* stiffness in OA bone [36, 37]. However, this hypothesis has not yet been tested.

2.4 FEM studies

FE modeling is an effective method to capture the relative and combined effect of OA-related structural alterations in different layers of the subchondral bone on the overall structural stiffness of the bone. The FE method is a numerical technique for finding approximate solutions to systems of partial differential equations (PDE) governing mechanical behavior of a structure. Using this method a complex structure can be divided into a finite number of smaller elements which can be solved in relation to each other. FE method provides great advantages in analyzing models with complex geometry and handling variable mechanical properties. Using this numerical method—unlike the experimental procedures that may require a number of specimens and experimental setups—different geometries and mechanical properties can be modeled with

time and cost efficiency. Also, obtaining experimental measures such as stress/strain values at points inside a sample can be very complicated, which is a much easier process using FE modeling.

FE analysis has been used in a few studies to evaluate the effect of OA related subchondral bone stiffening on cartilage stresses [23, 60]. Two other FE studies have evaluated load transmission patterns within the proximal tibia [22, 61]. With regards to hypotheses suggesting subchondral bone stiffening effecting stresses within overlaying cartilage layer [10], a plane-strain FE model of a simplified synovial joint was developed [60] (Figure 2-5). This modeling was done parallel to an animal study (sheep knee model) to investigate the effect of induced localized subchondral bone stiffening on cartilage stresses. In this study, subchondral bone stiffening 1-2 mm beneath the articular cartilage was induced using a cylindrical metal insert. The results of this research showed that subchondral bone stiffening increased the stresses within the overlaying cartilage layer by up to 50%. This FE model, however, was based on an oversimplified geometry of the subchondral bone [60], and eliminated the potential effects of bone geometry on stress distribution alterations. The method used to model subchondral bone stiffening was based on the parallel animal study and did not reflect actual OA-related subchondral bone stiffening. In addition, to determine the stress transmission effect of the subchondral bone stiffening, an indentor was used to apply load on the articular cartilage surface which did not match the real-life loading condition in the knee joint (Figure 2-5).

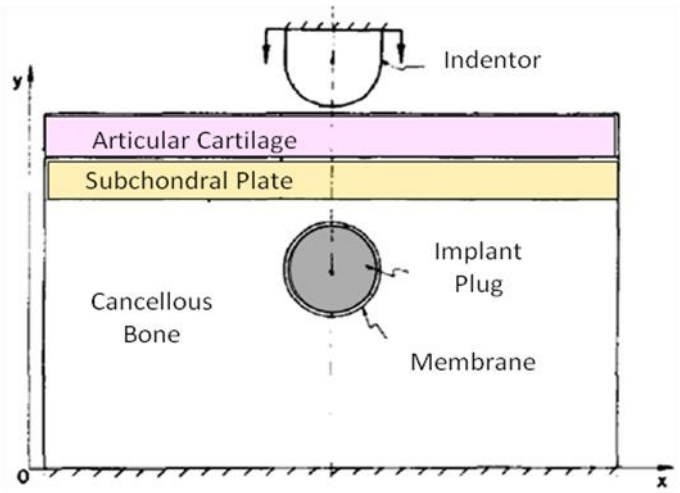

Figure 2-5) A plane strain simplified FE model of the subchondral bone and overlaying cartilage [60]. Local subchondral bone stiffening is modeled using a cylindrical metal implant beneath the subchondral cortical bone. Modified from Brown et al [60] with permission from Elsevier.

Another study, using a parametric axisymmetric FE model of an idealized synovial joint, attempted to determine the effect of altered stiffness and thickness of cartilage, calcified cartilage, subchondral cortical, and trabecular bone on the generated stresses within each layer [23]. The geometry of the joint was assumed to be comprised of a semi-sphere on a flat surface (Figure 2-6). The results of this study suggested that the subchondral bone mechanical properties have negligible effects on the stresses within the cartilage [23]. The cartilage thickness and stiffness alterations were shown to affect the stresses within the cartilage layer and other subchondral bone layers; but the mechanical properties of each subchondral bone layer affected only the stresses within itself and did not have significant effect on the stresses in other layers [23]. This study, however, used an idealized model of the joint which excludes the effects of the bone geometry on the relative effect of different layers on cartilage stresses. Furthermore, although the subchondral trabecular and epiphyseal trabecular bone are affected differently by OA, these tissues have not been discriminated from each other in this study. The stress distribution pattern has not been reported in this study; instead, the minimum and maximum

values for von Mises stress were taken as main outcomes of the study. However, as previously discussed, load transfer patterns may partially explain OA-related alterations of the subchondral bone layers.

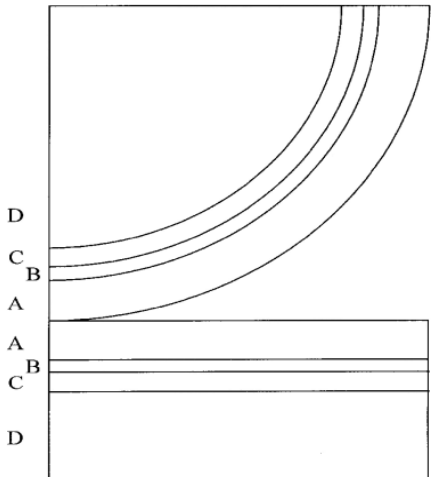

Figure 2-6) The axisymmetric FE model of an idealized synovial joint with the following layers: A, articular cartilage; B, calcified cartilage; C, subchondral cortical bone; D, subchondral trabecular bone. From Dar and Aspden [23] with permission from SAGE.

To study the load transmission mechanism in the bone, (Figure 2-7 A&B) researchers have used 3D [61] and axisymmetric [22] FE models of the proximal tibia. One study developed a 3D FE model of the proximal tibia to be used for further research in field of knee implants [61]. The researchers used principal compressive stress flow and safety factor numbers at the trabecular and cortical bone to validate their models with the actual trabecular orientation in the proximal tibia and bone strength. Another study used an axisymmetric FE model of the proximal tibia [22] to study the load transfer pattern inside the bone, correlating stress flow and trabecular orientation inside the bone. However, these studies did not assess OA-related bone alterations, and were based on one set of normal bone mechanical properties and geometry with no altering parameters.

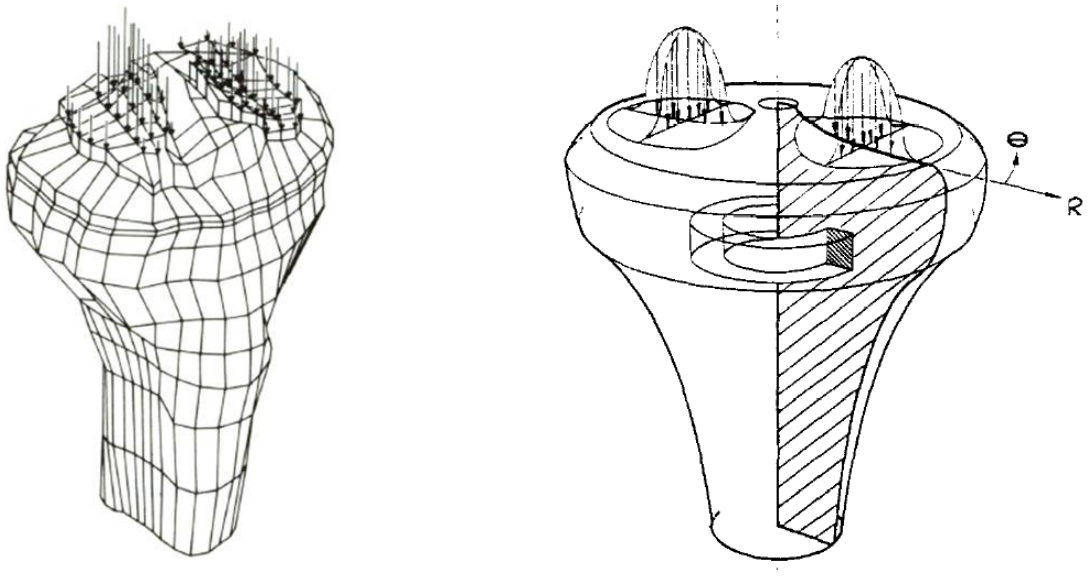

A. B.

Figure 2-7) A. 3D FE model of the proximal tibia to study the stress patterns within the bone, from Little et al [61]. B. Axisymmetric FE model of the lateral proximal tibia to study the load transmission mechanism in the proximal tibia, from Hayes et al [22] with permission from Elsevier.

Currently, there is a lack of FE research using image-based geometry of the proximal tibia to determine the structural effects of OA-related altering stiffness and thickness of different subchondral bone layers. Using this FE model, one can study the contribution of each subchondral bone layer on the overall stiffness of the bone and the load transmission mechanism inside the bone. These parameters, and their correlation with OA-related morphologic and mechanical alterations, will improve our understanding of the role of subchondral bone in OA initiation and progression.

2.5 Summary

1. The role of subchondral bone in OA initiation and progression is unclear. Major hypotheses suggest that mechanical and morphological alterations in subchondral bone are drivers of OA progression.
2. The limited number of human studies on subchondral bone mechanical and morphological properties has shown that different layers of subchondral bone (subchondral cortical, subchondral trabecular and epiphyseal trabecular bone), lying in different depths from the subchondral surface, are affected differently by OA.
3. Most OA research in this area has focused on isolated tissues (e.g. only subchondral cortical bone), disregarding the effect that combined alterations in different subchondral bone layers might have on the overall structural stiffness of the bone.
4. FE analysis is a non-invasive tool which has potential to be used to study the effect of OA-related alterations in different layers of the subchondral bone on overall mechanical and structural behavior. However, there are few FE studies focusing on OA subchondral bone and no model has been used to assess the relative and combined effect of different subchondral bone mechanical and morphologic properties on overall stiffness of the bone.

3 Research Questions and Objectives

The fundamental question which motivates my thesis research is: What is the mechanical role of subchondral bone in the initiation and progression of OA? To help answer this fundamental question, the goal of my study was to develop FE simulations of OA bone. Using FE modeling, I aimed to answer the following research questions:

1. What are the relative and combined influences of osteophyte formation and subchondral cortical, subchondral trabecular and epiphyseal trabecular bone morphological and mechanical alterations on overall bone stiffness?
2. What are the effects of osteophyte formation and altering subchondral cortical, subchondral trabecular and epiphyseal trabecular bone thickness and stiffness on load transmission mechanism in the proximal tibia?

To answer the above research questions, the specific objectives to be achieved include:

1. Develop a parametric finite element model of a typical proximal tibia.
2. Determine individual and combined effects of OA-related osteophyte formation and morphological and mechanical changes to subchondral and epiphyseal bone on overall bone stiffness.
3. Determine how OA-related bone alterations affect load transmission in the OA proximal tibia.

4 Methods

4.1 FE Model Development

4.1.1 Material and Morphologic Tissue Properties

The following parameters have been reported to be affected by OA in the proximal tibia: osteophyte diameter (OD) and thickness and stiffness (elastic modulus) of bone regions below cartilage, defined as subchondral cortical thickness (SCT), subchondral trabecular thickness (STT), subchondral cortical stiffness (SCS), subchondral trabecular stiffness (STS), epiphyseal trabecular stiffness (ETS) [7, 8, 11, 14, 43, 62-67]. For each parameter, a range of variations has been reported for both normal and OA bones [8, 13, 23-25, 38, 40-43, 47, 51-53, 68-71], and these values are summarized in Tables 4-1 to 4-5. We assigned a typical value for each parameter representing bone properties unaffected by OA using the average and/or median values reported in literature for the normal proximal tibia [8, 13, 23-25, 38, 40-43, 47, 51-53, 68-71] (Table 4-6). The typical elastic moduli of the diaphyseal cortical and metaphyseal trabecular bone in the model were chosen as 14000 MPa and 200 MPa, respectively, and the Poisson's ratio for bone and cartilage were assigned as 0.3 and 0.4, respectively [23-25, 38].

Table 4-1) Compilation of studies reporting subchondral cortical thickness (SCT) of normal and/or OA proximal tibia and femoral head. Proximal tibial studies are listed chronologically. Femoral head studies are listed last. The widest range and the weighted average (weighted using the sample size of each study and the corresponding median value) for each type of bone are reported at the end of the Table based on the data for the proximal tibia.

Reference year	**Bone site**	**Samples/ Specimens**	**Methods**	**Parameter (mm)**	**Parameter type**		
					Normal	**OA**	**Pooled**
Clark and hubber 1990	Proximal tibia	20	Histology	SCT			0.1-3
Milz and Putz 1994	Proximal Tibia	24	Histology	SCT	0.1–1.5		0.02-2.1
Yamada et al 2002	Proximal Tibia	72/140	Histology Radiography	SCT	1.1-4.8	1.3-4	
Buckland Wright 2004	Proximal tibia/ Femoral head	64	Radiography	SCT	0.31-0.43	0.42-0.92	
Grynpas MD. 1991	***Femoral head***	*38*	*Histomorphometry*	*SCT*	*0.2-0.55*	*0.25-0.85*	
	Widest range				***0.1-4.8***	***0.42-4***	***0.02-3***
	Average				***2 mm***	***2 mm***	***1.3 mm***

Table 4-2) Compilation of studies reporting subchondral cortical stiffness (elastic modulus) (SCS) of normal and/or OA proximal tibia and femoral head. Proximal tibial studies are listed chronologically. Femoral head studies are listed last. The widest range and the weighted average (weighted using the sample size of each study and the corresponding median value) for each type of bone are reported at the end of the Table based on the data for the proximal tibia.

Reference (year)	**Bone site**	**Samples/ Specimens**	**Methods**	**Parameter (MPa)**	**Parameter type**		
					Normal	**OA**	**Pooled**
Brown 1984	Proximal tibia	Lit. Rev.		SCS	2070-13800		
Little 1986	Proximal tibia	Lit. Rev.	Lit Rev	SCS	17200		
Choi et al 1990	Proximal tibia	1/20	3 point bending	SCS	600-1900		
Li and Aspden 1997	***Femoral head***	*23*	*Ultra-sound*	*SCS*	*13500-20000*	*8300-18500*	
	Widest range				***600-17200***		
	Weighted Average				***2920 MPa***		

Table 4-3) Compilation of studies reporting subchondral trabecular stiffness (elastic modulus) (STS) of normal and/or OA proximal tibia and femoral head. Proximal tibial studies are listed chronologically. Femoral head studies are listed last. The widest range and the weighted average (weighted using the sample size of each study and the corresponding median value) for each type of bone are reported at the end of the Table based on the data for the proximal tibia.

Reference (year)	**Bone site**	**Samples/ Specimens**	**Methods**	**Parameter (MPa)**	**Parameter type**		
					Normal	**OA**	**Pooled**
Brown 1984	Proximal tibia	Lit. Rev.		STS/ETS	34.5-690		
Little 1986	Proximal tibia	Lit Rev	Indentation test	STS	150-400		
Bentzen et al 1987	Proximal tibia	3/165	Platen	STS	6-1670		
Finlay et al 1989	Proximal tibia	28	Indent inverse	STS	162-501	64-530	
Zysset et al 1994	Proximal tibia	4/160	platen	STS	135-707	60-707	
Ding et al 1998	Proximal tibia	19/114	platen	STS/ETS	23-887	53-646	
Ding et al 2001	Proximal tibia	20/120	platen	STS/ETS	187-693	211-339	
Li and Aspden 1997	***Femoral head***	*23*	*Platen*	*STS/ETS*	*41-460*	*118-551*	
	Widest range				***6-1670***	***53-707***	
	Weighted Average				***495 MPa***	***337 MPa***	

Table 4-4) Compilation of studies reporting subchondral trabecular stiffness (elastic modulus) (STS) of normal and/or OA proximal tibia and femoral head. Proximal tibial studies are listed chronologically. Femoral head studies are listed last. The widest range and the weighted average (weighted using the sample size of each study and the corresponding median value) for each type of bone are reported at the end of the Table based on the data for the proximal tibia.

Reference (year)	**Bone site**	**Samples/ Specimens**	**Methods**	**Parameter (MPa)**	**Parameter type**		
					Normal	**OA**	**Pooled**
Brown 1984	Proximal tibia	Lit. Rev.		STS/ETS	34.5-690		
Keyak et al 1994	Proximal tibia	4/36	Platen	ETS	36-2767		
Zysset et. al 1994	Proximal tibia	4/160	platen	ETS	198-825	222-897	
Ding et. al 1998	Proximal tibia	19/114	platen	STS/ETS	23-887	53-646	
Day et al 2001	Proximal tibia	20		STS/ETS	280-1080	130-650	
Ding et. al 2001	Proximal tibia	20/120	platen	STS/ETS	187-693	211-339	
Morgan et al 2003	Proximal tibia	15/15	Platen	ETS	10-2770		
Li and Aspden 1997	***Femoral head***	*23*	*Platen*	*STS/ETS*	*41-460*	*118-551*	
	Widest range				***10-2767***	***53-897***	
	Weighted Average				***570 MPa***	***411 MPa***	

Table 4-5) Compilation of studies reporting the morphologic and mechanical properties of the proximal tibia except the previously listed parameters of subchondral cortical thickness (SCT), subchondral trabecular thickness (STT), subchondral cortical stiffness (elastic modulus) (SCS), subchondral trabecular stiffness (STS), and epiphyseal trabecular stiffness (ETS).

Reference (year)	Bone site	Samples/ Specimens	Methods	Parameter	Parameter type		
					Normal	OA	Pooled
Brown 1984	Proximal tibia	Lit. Rev.		Cartilage S (MPa)	3.45-20.7		
				Cartilage Poisson's	0.47		
				Cortical wall S (MPa)	13800		
				Bone Poisson's	0.3		
Little 1986	Proximal tibia	Lit Rev	Lit Rev	Cartilage S (MPa)	11.6		
				Cartilage Poisson's	0.4		
				SC Poisson's	0.3		
Zysset et. al 1994	Proximal tibia	4/160	platen	Metaphyseal trabecular stiffness (MTS) (MPa)		200-1800	
Dar and Aspden 2003	Burr 1998			Cartilage T (mm)			1-5
				Cartilage S (MPa)			20-750
				SC Poisson's			0.2-0.4
				ST Poisson's			0.2-0.4
				Cartilage Poisson's			0.2-0.485

Table 4-6) Variation range and typical values for the morphological and mechanical properties of the proximal tibia used in the parametric FE model (the typical value represents an unaffected normal bone, and the range of variation includes the values reported for normal and OA proximal tibiae).

Property	Variation Range	Typical value	Reference
Osteophyte Diameter (OD)	0-12 mm	NA	[72]
Subchondral Cortical Thickness (SCT)	0.1-4.8 mm	2 mm	[23, 47, 51-53]
Subchondral Cortical Stiffness (SCS)	600-17200 MPa	3000 MPa	[23, 60, 61, 69]
Subchondral Trabecular Thickness (STT)	1-4 mm	2.5 mm	[13]
Subchondral trabecular Stiffness (STS)	6-1670 MPa	500 MPa	[23, 38, 41-43, 60, 61, 70]
Epiphyseal Trabecular Stiffness (ETS)	10-2767 MPa	500 MPa	[38, 40-42, 60, 71, 73]

4.1.2 Proximal Tibial Shape

To derive proximal tibial shape, segmented computed tomography (CT) images of 16 male cadaveric tibia used in previous studies [2] were analyzed. These specimens came from 10 consenting donors (8 males and 2 females; ages ranging from 67 to 88 years (mean ± standard deviation (SD): 77.8 ± 7.4)) and included six left:right pairs, two right and two left knees with 6 subjects identified with OA. The average overall volume of the proximal tibia and the average medial and lateral compartment areas of the samples were derived using custom algorithms. The sample with the closest overall volume and medial/lateral compartment areas to the average values was selected for the FE model. The selected sample was from a knee with early OA (KL grade = 1). The midcoronal section of the proximal tibia containing subchondral cortical and trabecular layers in both medial and lateral compartments was selected to develop a parametric 2-dimentional (2D) FE model (Figure 4-1 A). The outer boundary (Figure 4-1 B) and the subchondral cortical, subchondral trabecular, and epiphyseal trabecular layer boundaries were estimated and segmented using commercial image processing software (Analyze, Mayo Foundation) (Figure 4-1 D). The subchondral cortical thickness along the periphery of the proximal tibia, the common site of osteophyte formation, is reported to have 0.1 – 0.3 mm thickness [52]. In this model a conservative peripheral thickness of 0.3 mm was used.

Semi-circular bony regions, located at the peripheral edge of the proximal tibial subchondral cortical bone, were added to the normal model to simulate osteophyte formation. Four different diameters of 3, 6, 9 and 12 mm for the osteophyte diameters were used for the FE model. The 6 mm diameter osteophyte represents the average size of the OA related osteophyte [72].

The coordinates of the boundary points were defined using custom algorithms (MATLAB, MathWorks Inc.) (Figure 4-1 C) and input into commercial FEA software (ANSYS Academic Research, Release 11.0, ANSYS Inc.) to produce a 2D outline of the proximal tibia and its different layers.

The cartilage layer was created in FE software using the overall shape of the articular cartilage covering the lateral compartment of the proximal tibia seen in sample MRI images of human cadaveric bones. The thickness of this layer at the thickest site (middle of the lateral compartment was set to 3 mm based on MRI images of the proximal tibial midcoronal section and literature [23].

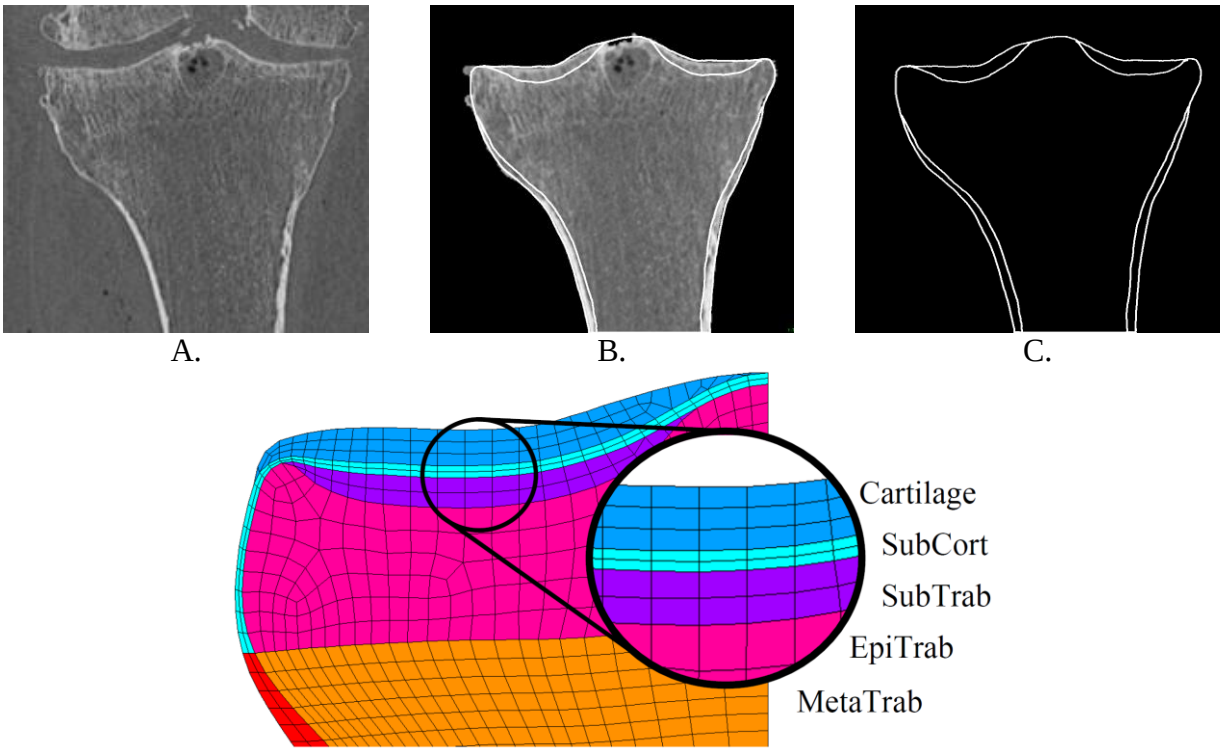

Figure 4-1) A. Mid-coronal CT-scan image of a human cadaveric proximal tibial sample, B. Outer geometry and boundaries of the bone layers were segmented in the CT image, C. The coordinates of the boundary points were identified using an in-house developed image processing code to import into FEA software, D. The different regions in a portion of the FE model (each color represents different material properties).

4.1.3 FE Modeling

To simplify the model and avoid complications caused by the tibiofibular joint and differences in the medial/lateral load distributions, the lateral compartment of the bone was selected [22] and a symmetric 2D model was produced (Figure 4-1 D). A plane-strain 2D analysis approach was used to analyze the proximal tibia.

4.1.4 Meshing

The mesh of different proximal tibial regions was controlled to maintain a coherent transition from smaller element size at proximal regions of the model with layers of low thickness to larger elements in more distal parts of the model. The meshing process resulted in a total of 1080 elements (PLANE42 solid elements) (Figure 4-1 D).

4.1.5 Material Modeling

Material properties were treated as linear elastic and isotropic. The effect of anisotropy of trabecular bone is reported to be minor if heterogeneity of the material is taken into account [24]. This model accounted for heterogeneity by modeling the trabecular region as 7 different regions with different elastic moduli to simulate the material properties of different locations.

4.1.6 Boundary Conditions

The distal nodes of the model were constrained from vertical movement. Also according to symmetry conditions of the model, the nodes on the symmetry line were constrained from horizontal movement. The distal section of the diaphyseal cortical bone was modeled

perpendicular to the distal boundary of the bone in order to avoid any bending moments at this section (Figure 4-2 B).

4.1.7 Loading Conditions

The loading region on cartilage layer of the model was defined based on shape of loading area and the bone-cartilage contact area [74]. The length of the loading region in this 2D model was estimated to be 19 mm. The loading pattern was simplified to a uniform pressure distribution on this region and the magnitude of the pressure was taken from previous modeling approaches [24] (Figure 4-2 A). A pressure of 3.2 MPa was applied at the cartilage surface, based upon a joint load of 2450 N [24] applied across a contact surface of 1050 mm^2 [74].

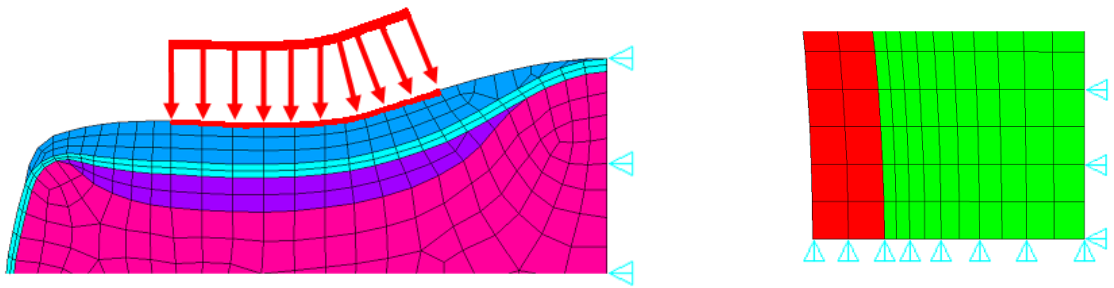

A. B.

Figure 4-2) A. Uniform pressure on the cartilage layer of the model based on contact area of the tibio-femural joint. B. Distal nodes constrained in vertical direction and the symmetry nodes constraind in horizontal direction.

4.2 Structural Stiffness

The effective stiffness (K) of the proximal tibia, measured directly at the subchondral bone surface, was defined using the total load applied to the model (P_{tot}) divided by the average

vertical displacement of the subchondral cortical surface nodes located underneath the loading region (U).

$$K = \frac{P_{tot}}{U}$$

4.3 Study Design

To determine the effect of osteophyte formation and changing morphologic and mechanical properties associated with OA on proximal tibial stiffness, the effect of individual changes in each parameter (OD, SCT, SCS, STT, STS, ETS) was determined. For each set of analyses, one parameter was altered within the range of values observed with OA while the other five parameters were set at normal values. Next, a combination of OA-related morphological and mechanical properties was applied to the model to assess the overall effect on stiffness. A reference 20% increase or 20% decrease of each parameter (except for OD), which is within range of values seen with OA [12, 59], was also used to assess the relative effect of mechanical and morphological changes on stiffness. For all test conditions, the resultant effective stiffness (K) was reported relative to the normal effective stiffness (K_{norm}) determined using typical normal knee values given in Table 6.

4.4 Load Transmission

To determine how OA-related bone changes affected load transmission patterns (secondary objective), we evaluated principal compressive stress contour plots (ANSYS Academic Research license) for the loaded normal bone and OA bone over variation range of different parameters. Stress contour plots provided visual representations of how load was transmitted from the

cartilage surface to the cortical diaphysis for the representative model with 6 mm osteophyte and 20% increase in SCT, SCS, STT, STS.

5 Results

Subchondral cortical and subchondral trabecular bone did not have dominant effects on the overall stiffness of the model (Figure 5-1). There was little variation of K/K_{norm} across the whole range of thickness and stiffness values observed with normal and OA bone (Figure 5-1 A-D). For example, K/K_{norm} varied between 0.99 and 1.045 for minimum/maximum SCT values of 0.5 and 2.0mm, respectively (Figure 5-1 A). This meant that if SCT doubled in thickness (from its original value of 1mm) the overall stiffness would only increase by 4.5%.

Epiphyseal trabecular bone stiffness had the most dominant effect on overall stiffness of the proximal tibia (Figure 5-1 F). There was large variation of K/K_{norm} across the range stiffness values observed with normal and OA bone (Figure 5-1 F). K/K_{norm} varied between 0.018 and 1.81 for minimum/maximum ETS values of 1 and 1000 MPa, respectively (Figure 5-1 F).

Simulating osteophyte formation by adding extra cortical bone to the peripheral edges of the model did not change the load transfer pattern from the articular surface through trabecular bone to the cortical diaphysis (Figure 5-2). Increasing the diameter of the osteophyte also did not markedly increase overall stiffness (Figure 5-1 E). A change in osteophyte diameter from 3 mm to 12 mm (4x bigger) only increased overall stiffness by less than 0.1% (Figure 5-1 E).

Isolated comparisons against a common reference (+/- 20% change from normal value) showed that epiphyseal trabecular bone stiffness had the most marked effect on overall stiffness. A 20% reduction in ETS resulted in a 11% reduction in overall stiffness (Table 2). Conversely, 20% increases in subchondral cortical or subchondral trabecular bone stiffness resulted in a 1% increase in overall stiffness (Table 2).

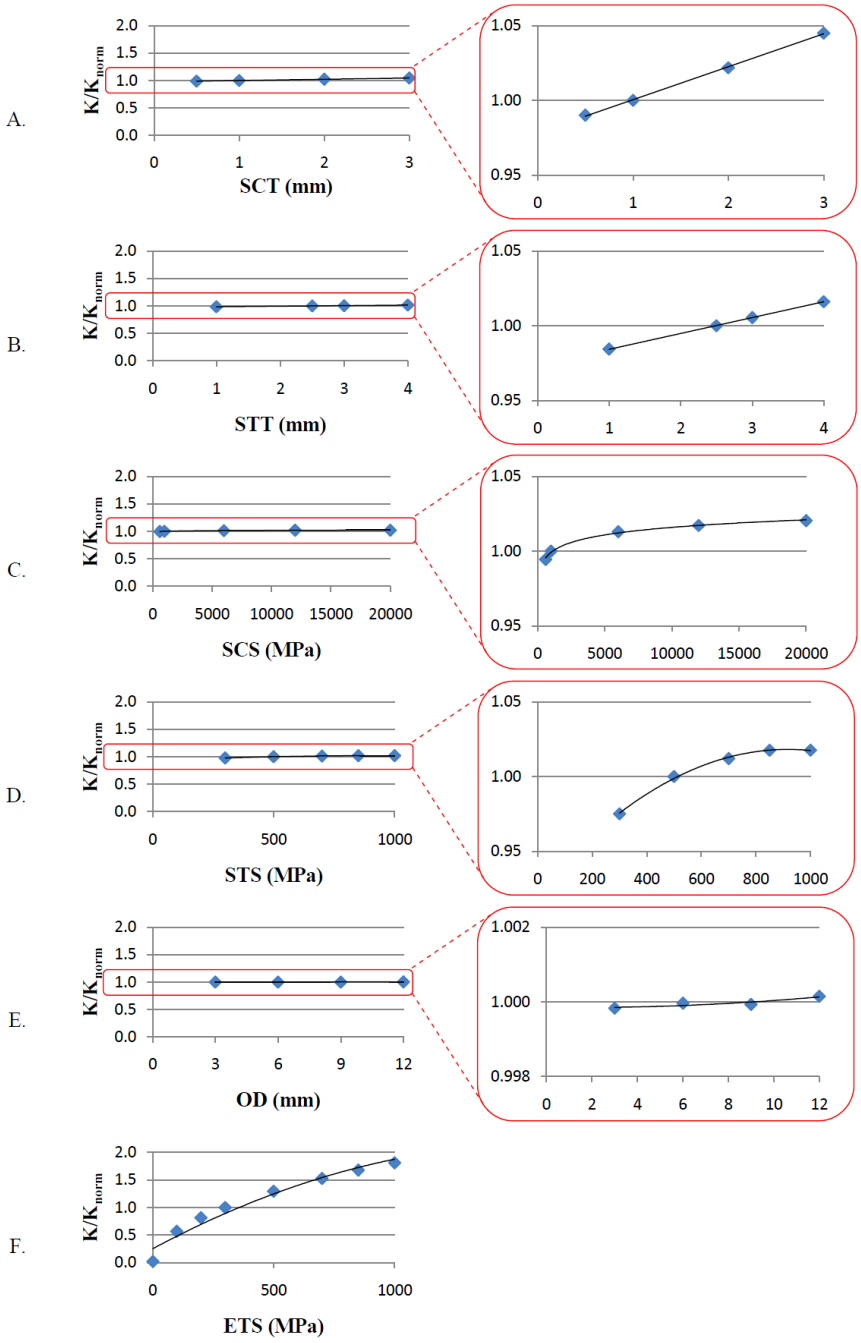

Figure 5-1) K/K_{norm} plotted relative to each parameter across its variation range (for different normal and OA proximal tibial bones). The studied parameters are: A. subchondral cortical thickness (SCT), B. subchondral trabecular thickness (STT), C. subchondral cortical stiffness (elastic modulus) (SCS), D. subchondral trabecular stiffness (STS), E. osteophyte diameter (OD), and F. epiphyseal trabecular stiffness (ETS).

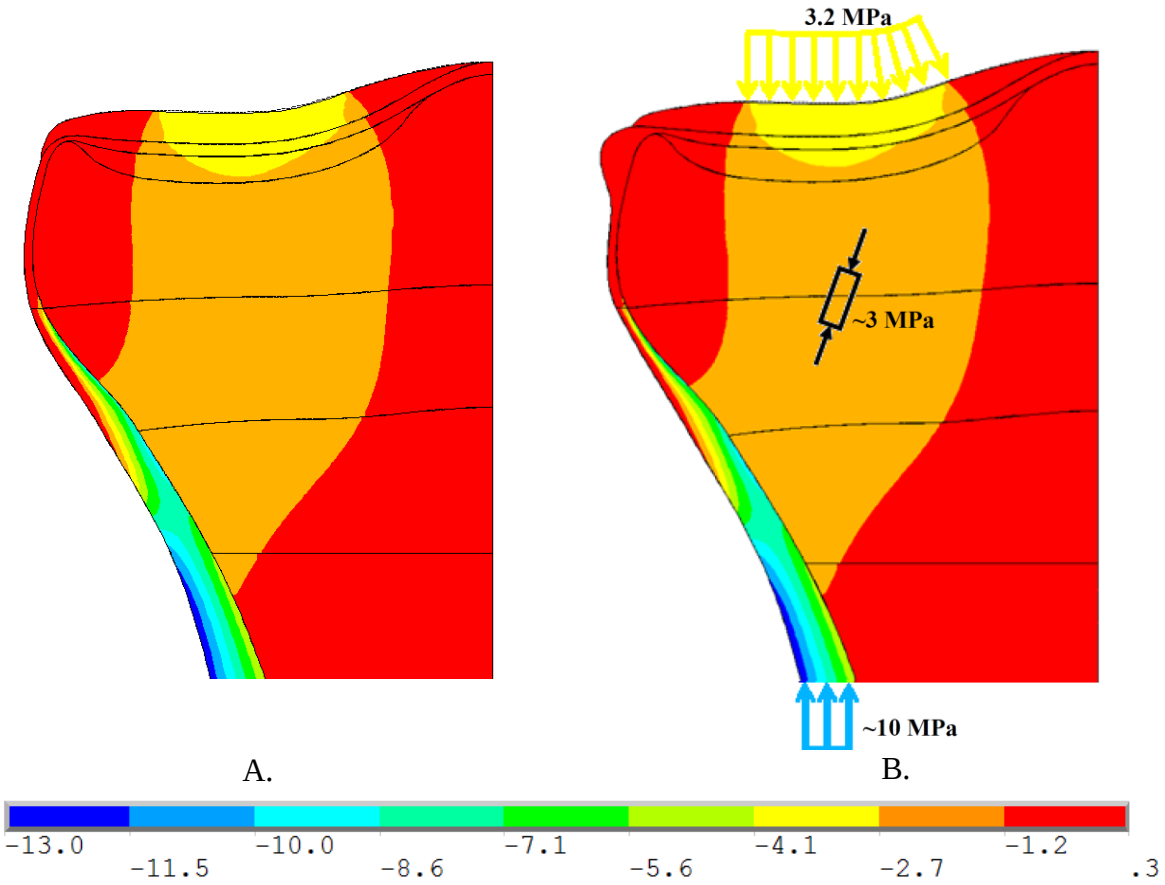

Figure 5-2) Minimum principal stress (compressive) contour for A. normal cortical thickness and B. 6 mm diameter osteophyte at the peripheral edge (to model the osteophyte formation effects) of the model with 20% increase in SCT, SCS, STT, STS, showing the load transfer pattern from the articular surface through trabecular bone to the cortical diaphysis. The undistorted stress pattern after osteophyte modeling demonstrates the little effect osteophyte formation in OA bone has on loading conditions in the proximal tibia.

The combined effects of osteophyte formation and increased thickness and stiffness of subchondral cortical and subchondral trabecular bone did not markedly increase overall stiffness (Table 3). Keeping ETS constant and increasing SCT, STT, SCS and STS by 20% resulted in only a 2% increase in overall stiffness (Table 3). Conversely, if ETS reduced by 20%, increases in SCT, STT, SCS and STS by 20% still resulted in a reduced overall stiffness of -9% magnitude (Table 3).

Table 5-1) Effect of altering each parameter on overall stiffness of the proximal tibial model. K/K_{norm} represents the change in K following ±20% variation of each parameter, with respect to its normal value (K_{norm}).

Parameter	**Typical**	**-20%**	**K /K_{norm}**	**+20%**	**K /K_{norm}**
SCT	2 mm	1.6 mm	1.00	2.4 mm	1.00
STT	2.5 mm	2 mm	1.00	3 mm	1.00
SCS	3000 MPa	2400 MPa	0.99	3600 MPa	1.01
STS	500 MPa	400 MPa	0.99	600 MPa	1.01
ETS	500 MPa	400 MPa	0.89	600 MPa	1.10

Table 5-2) Effect of altering multiple parameters on overall stiffness of the proximal tibia. The change in K following -20% variation of ETS and +20% variation of indicated group of parameters, with respect to its normal value (Knorm) is listed. For all analyses the 6 mm diameter osteophyte (representing an approximated average size for OA related osteophytes [72]) was included in the model.

-20%	**Normal**	**+20%**	**Osteophyte**	**K /K_{norm}**
	STS, SCS, STT, ETS	SCT	6 mm	1
	STS, STT, ETS	SCT, SCS	6 mm	1.01
	STS, ETS	SCT, SCS, STT	6 mm	1.01
	ETS	SCT, SCS, STT, STS	6 mm	1.02
ETS	SCS, STT, STS	SCT	6 mm	0.9
ETS	STT, STS	SCT, SCS	6 mm	0.9
ETS	STS	SCT, SCS, STT	6 mm	0.9
ETS		SCT, SCS, STT, STS	6 mm	0.91

6 Discussion

6.1 Overview of Findings

In this study we developed a 2D parametric FE model of a human cadaveric proximal tibia to determine the relative effects of varying morphological and mechanical properties of different bony layers on overall proximal tibial stiffness. This model is based on actual geometry of the bone and combines effect of different OA related alterations of bone properties on overall proximal tibial stiffness.

Our results show that the thickness and stiffness of the subchondral cortical and subchondral trabecular layers (SCS, SCT, STS and STT) had little effect on overall stiffness of the bone. These findings contradict theories proposing that increased stiffness and amounts of subchondral cortical and trabecular bone near the subchondral bone surface will result in an overall stiffer bone under the cartilage layer, leading to cartilage degeneration [8, 11]. Even with a 20% increase in both SCS and STS—as observed in late OA conditions [12]—the overall stiffness increased by only 1%. Even a 100% increase in any of these four parameters only increased stiffness by a maximum amount of 4.5%. The contrast between these findings and theories regarding increased stiffness of OA bone is likely due to lack of previous simultaneous assessment of all tissues (subchondral cortical/trabecular and epiphyseal trabecular) in the OA proximal tibia. In many OA related studies, only one isolated tissue has been focused on, and the corresponding variations in properties of other tissues have been ignored. Based upon our results, OA-related changes in subchondral cortical and trabecular bone stiffness and morphology are unlikely to considerably increase the overall stiffness of bone.

These results demonstrate that epiphyseal trabecular stiffness has the dominant effect on overall stiffness at the subchondral bone surface. These findings suggest that lower epiphyseal

trabecular bone density seen with OA [5, 15, 19], which can be interpreted as lower epiphyseal trabecular stiffness [75], results in an overall *weaker* proximal tibial bone. Weaker trabeculae in epiphyseal trabecular bone and subchondral trabecular bone are likely to crush under loading, which may explain OA-related observations of sclerosis and higher apparent BMD via using Dual-Energy X-ray Absorbtiometry (DXA) and CT [7, 43, 62, 64, 76]. This theory is in agreement with previous findings about random trabecular orientation in areas near subchondral bone [9]. The crushed bone, despite having a higher density, is weaker than normal subchondral trabecular bone and results in an overall weaker bone structure. Importantly, the weaker bone supporting the articular surface will affect the load and stress distributions in cartilage differently than in normal conditions, so OA-related bone changes in epiphyseal trabecular bone may still be related to cartilage degeneration.

Our results also show that the presence of osteophytes at the peripheral edge of the proximal tibia has little effects on the overall stiffness and load transmission pattern of the bone. These findings contrast with the idea that osteophytes located on peripheral edges of the OA proximal tibia increase the structural stiffness of the bone [21, 77].

Rationale on why epiphyseal trabecular bone has the dominant effect on overall stiffness is due to geometry of the proximal tibia. In both the normal and OA proximal tibia, load is primarily transmitted through subchondral cortical bone through trabecular regions to the metaphysis and cortical diaphysis. Due to the thin thickness of cortical bone along the periphery, less load is transmitted along the peripheral cortical edges of the structure to the cortical diaphysis. Thus, overall stiffness of the proximal tibia is mediated by the stiffness of the weakest structure (epiphyseal trabecular bone). Even osteophytes with diameters as big as 12 mm (twice the average value) at the peripheral edge of the proximal tibia with maximum values for SCT,

SCS, STT, STS results in a little increase in the overall stiffness (<0.1%) and little alteration of load transmission pattern. This observation suggests that the stress shielding theory is highly unlikely. A more reasonable scenario would be that epiphyseal bone changes occur before overlying subchondral bone changes (as observed in animal models of OA [15, 19]), resulting in a weaker structure, subsequent failure of trabecular bone, and observed sclerosis.

6.2 Comparison to Existing Findings

Our results compare favorably with previous FE analyses. The compressive stress flow pattern from the articular surface of the proximal tibial model to the metaphyseal cortical bone obtained from our FE analysis is in agreement with previous FE models of the proximal tibia [22, 24] (Figure 6-1). Also, the site and value of the maximum compressive stress in our model is in agreement with previous analyses using similar loading conditions [24].

Figure 6-1) Maximum compressive stress site and value of my proximal tibial FE model (on the right) are in close agreement with literature [61] (on the left) using similar loading conditions.

6.3 Strengths and Limitations

Major strengths of this study pertain to usage of a parametric FE modeling approach and a model simulating actual geometry of the proximal tibia. First, our parametric FE modeling approach enabled us to take thickness and stiffness alterations into account, and determine the relative effect of each parameter on overall stiffness of the model. This is particularly important for OA proximal tibiae where concurrent variation of a group of parameters makes it difficult to investigate the individual effect of each parameter practically. This is an effective approach to study the overall effect of OA-related bone changes directly at the highly relevant subchondral bone surface. Second, our model was based upon actual physical geometry of the proximal tibia. This is an important approach to mimic realistic loading and boundary conditions at the proximal tibia. Conversely, an oversimplified geometry (e.g. flat surface, circular layers, etc.) [23, 25], may change the mechanical behavior of the model, to some extend that conclusions regarding load transmission and the effects of altered morphological and mechanical properties on overall stiffness would be questionable.

For our study we used a 2D plane-strain symmetric model of the lateral compartment with linear elastic homogeneous isotropic material properties to simulate the proximal tibia. This modeling requires some comments. First, both the plane strain and plane stress models give similar results, however, considering the geometry of the proximal tibia, plane strain approach was more suitable for this analysis. The other option was to use an axi-symmetric model. It was not selected because 1) loading in the proximal tibia occurs only on two semi-parallel regions of the bone (not circularly distributed over the articular surface), and 2) load transfer patterns obtained from preliminary axi-symmetric models were not compatible with literature results [22, 24]. Second, the selected symmetric modeling approach only neglects some small non-

symmetries in the shape and loading of the real bone. The main non-symmetric feature of the proximal tibia is the presence of fibula, attached to the lateral compartment of the proximal tibia, which supports the bone in this region. This may alter the loading behavior of the tibia which was not included in the symmetric FE model, and might be an area for possible future work. Third, the lateral compartment selection was in agreement with previous FE study of the proximal tibia [22], thereby permitting comparison and validation of results with published findings. However, OA hallmarks (such as cartilage degeneration) are primarily located in medial compartment, in which, the load transmission mechanism may be different. Studying the probable differences caused by using the medial compartment in a FE analysis similar to the present model is an area for future research. Fourth, linear elastic assumptions for material properties was selected because this approach is considered valid for modeling bone, which does not exhibit large deformations or a time-dependent material behavior [78]. Fifth, as the loading is mostly along the long axis of the bone, homogeneous isotropic material properties are valid for subchondral cortical and trabecular layers with little effect on the results [79]. However, to partially account for the non-homogeneouity that exists in the trabecular region, this area was divided into 7 different sub-regions with different homogeneous material properties assigned for each sub-region.

Our analysis has potential sources of error related to mesh size and determination of overall proximal tibial stiffness. First, the sensitivity of the FE model to mesh size was tested by applying different meshes with decreasing element sizes until the result would differ less than 2%, concluding that the analysis was independent of mesh size. Second, effective stiffness (K) was defined based on the average vertical displacement of the nodes located on the subchondral cortical bone under the loading region of the cartilage. There was some variation in vertical

displacement (which may affect K results), however, it was small (~5%). Also, the horizontal displacements of the nodes were small (<2% of the vertical displacement). Thus, the usage of the average vertical displacement was considered to be a justified approach for determining stiffness.

7 Conclusions and Future Directions

7.1 Conclusions

Our results suggest that:

1. Osteophyte formation and OA related subchondral cortical and subchondral trabecular bone morphology and mechanical properties alterations have little effect on overall stiffness of proximal tibial subchondral bone.
2. Epiphyseal trabecular bone stiffness is the dominant contributor to the overall proximal tibial stiffness.
3. Our results suggest that observed differences between OA and normal bone morphology and mechanical properties may contribute to OA bone being weaker and more flexible than normal bone, not stiffer.

7.2 Contributions

Using the parametric FE model of the proximal tibia, we were able to apply various scenarios with different values for the parameters based on the reported OA related morphologic and mechanical properties alterations and study the resultant overall effect on the proximal tibial bone stiffness. This is the first parametric FE model of the proximal tibia based on imaged bone geometry and the first FE modeling study to assess the combined effect of different OA related alterations of bone properties on overall proximal tibial stiffness. Our results show that the epiphyseal trabecular bone stiffness (compared to subchondral cortical an trabecular stiffness/thickness) has the dominant effect on the overall stiffness of the proximal tibia. This analysis was important because it included the combined effect OA related morphologic and mechanical properties alterations on the proximal tibia rather than focusing only on individual parameters. Without this information we would not be able to determine the relative effect of

different parameters involved in initiation and progression of the OA, which may mislead researchers in finding an effective diagnosis method or cure for OA.

7.3 Clinical Significance

Currently there is no cure for OA and its exact cause is unknown. The lack of early diagnostic methods has made it impossible to detect the disease early enough for successful clinical intervention. As a result, OA is usually detected after significant cartilage damage and bone distortion. Determining the most affected bone tissue by OA would help to narrow research foci and help identify disease onset. Also, as most "cure" strategies for OA focus on cartilage damage or subchondral cortical and subchondral trabecular bone alterations, introducing the epiphyseal trabecular bone as a dominant factor in defining proximal tibial overall stiffness may indicate the necessity of targeting this tissue to prevent OA progression.

7.4 Recommendations for Future Research

The FE model used in this study has some potential for improvement, which is discussed in this section. A number of revised FE models (currently in a preliminary state) have been developed during the course of this research, to account for limitations with the main model. These models can be used in future FE analyses to study the OA proximal tibia.

7.4.1 Loading conditions

7.4.1.1 Load distribution

The stress distribution within the cartilage layer and the underlying bone layers is associated with the load transmission profile at the cartilage layer. Deviations in this profile might alter the stress

distribution pattern in these layers. A different load flow path within the bone may, in turn, change the relative effect of different mechanical and morphological parameters on the overall bone stiffness.

In our current model, the loading condition was assumed as a constant pressure at a line representing the loaded region on the cartilage surface. The constant pressure assumption was a simplification of the actual load distribution on the cartilage layer. In reality, the loading profile on the cartilage might vary along the cartilage layer due to femur bone curvature and the presence of the menisci around the contact area of the cartilage. To account for this limitation, a 2D symmetric FE model of a typical total human knee was developed using QCT and MRI images of the human knee and the morphologic and mechanical properties reported in the literature for different compartments of the knee (Figure 7-1). Meniscus, cartilage layers and distal femur bone have been included in this model. To avoid the contact surface modeling complications, these sections have been modeled as being attached to the proximal tibial cartilage layer. Orthotropic mechanical properties have been assigned for the meniscus [80] and isotropic homogeneous material properties have been chosen for the cartilage layer (Table 4-5). By using the distal femur to apply load to the cartilage layer, this model offers an improved and more realistic loading condition, and also a more valid stress distribution within the cartilage layer.

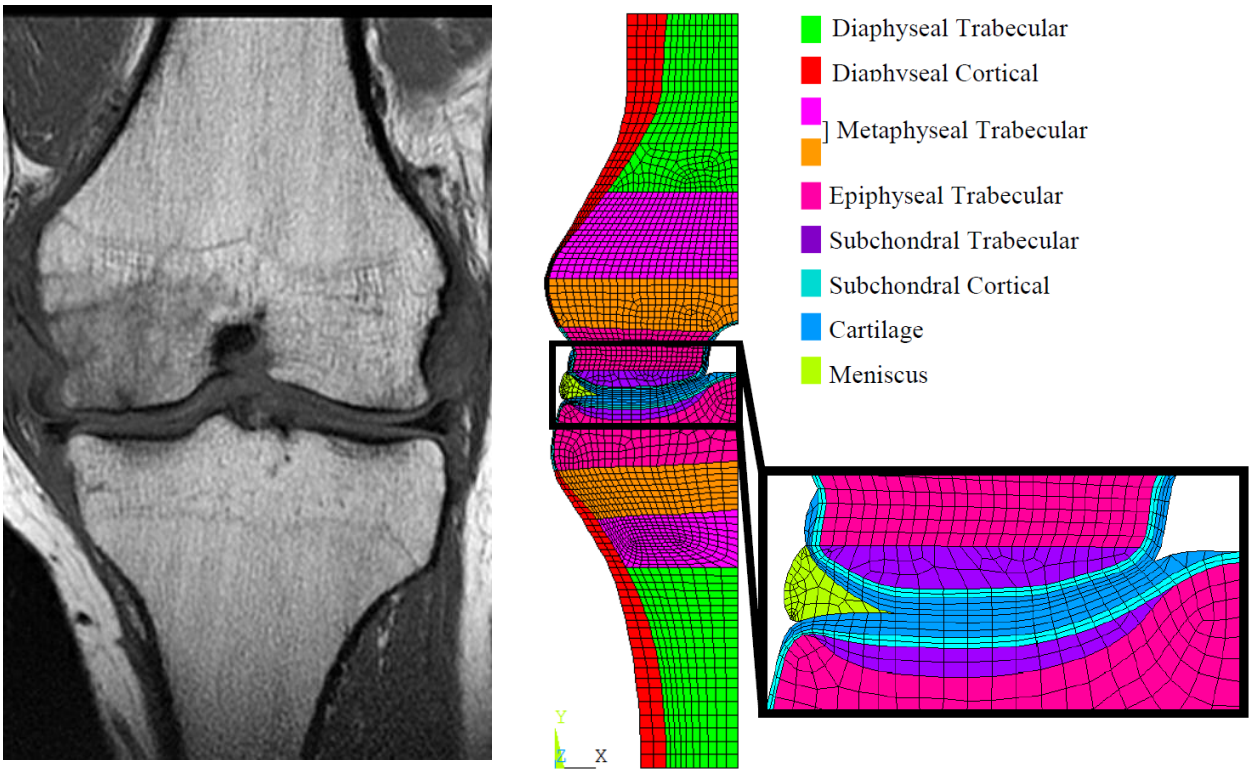

Figure 7-1) On the left, a sample MRI of the knee joint showing the distal femur, proximal tibia, articular cartilage layers and menisci. The lighter pixels show higher water content in the tissue. On the right, the symmetric FE model of the knee joint.

Preliminary results show that a 20% increase in SCT, SCS, STT and STS increases the overall stiffness of the proximal tibia on its subchondral surface (using total load applied on the proximal tibia and the average vertical deflection of the loaded region on subchondral surface) by 1.9% for the current model and 1.5% for the full knee model. Preliminary results also show that the vertical component of the load on the tibial cartilage surface represents an almost constant pressure profile on the region where there is direct cartilage on cartilage contact between the distal femur and proximal tibia (Figure 7-2). However, there is sudden change in the loading profile in the area of cartilage covered by meniscus. This abrupt change might be a result

of modeling the meniscus and cartilage layers attached to each other, with no relative motion allowed between the cartilage and meniscus surface (Figure 7-2).

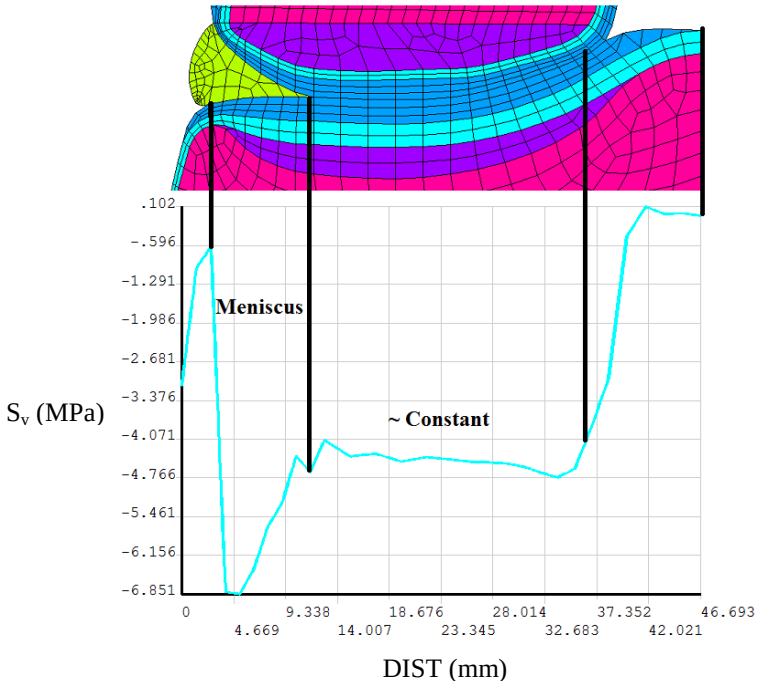

Figure 7-2) The vertical load component (S_y) on the surface of the tibial cartilage in terms of the distance from the tibial cartilage starting point on the lateral side of the bone towards the symmetry line. The cartilage-on-cartilage contact section covers the DIST= 10 mm to 35 mm. The negative values mean compressive loading condition.

To obtain a more realistic loading condition, modeling separate distal femur and menisci with contact elements on the contact surfaces of the tibial and femoral cartilage, and also the menisci, would be helpful. Also, allowing the meniscus to slide between two cartilage surfaces under loading would increase the accuracy of the model.

7.4.1.2 Loading rate

The main objective of this study was to determine the individual and combined effects of different parameters on overall stiffness of the bone. The overall stiffness of the bone, from its

definition, is independent of the amount of applied load and is a function of stiffness and geometry of the material. Also, as the material properties of all tissues in our model are considered to be elastic, their material stiffness is also independent of loading conditions (i.e., rate of loading). These reasons validate our main results regarding the relative effect of parametric alterations on the overall stiffness of the bone. However, in viscoelastic materials such as bone and cartilage, the material stiffness (E) is a function of loading rate. In such materials, the higher the loading rate, the larger the material stiffness would be. In addition, the amount of stresses within the subchondral bone layers and the cartilage depend on the amount of load and vary with altering loading conditions. In order to improve our FE models for purpose of studying the stresses within the cartilage layer, the load transmission pattern, and amount of load going through each section of the bone, impact loading conditions could be used to replace static loading conditions. The loading rate and variation profile during different physiological activities are available in gait analysis studies. These profiles could be imported in ANSYS/ABAQUOS and applied on the FE model.

7.4.1.3 Load transmission

As discussed previously, there are a number of hypotheses relating osteophyte formation and mechanical and morphological alterations in epiphyseal bone region to the stress shielding theory and load transmission pattern inside the bone. To test these hypotheses, it is important to study the load transmission mechanism of the bone in order to determine the stress flow within different layers of the bone and effects of different parameters on the stress pattern.

To obtain an in-depth understanding of the load transfer pattern along the proximal tibia from articular surface of cartilage through the subchondral and epiphyseal trabecular regions to the cortical diaphysis, a modified model of the proximal tibia was developed using beam

elements instead of plane elements in the peripheral cortical shell and cortical diaphysis. This model can be used to obtain the bending moment distribution and shear stress variations along the proximal tibia, besides the stress contours inside different layers of the bone, and can be used to help determine the effect of each parameter on load transfer pattern (Figure 7-3).

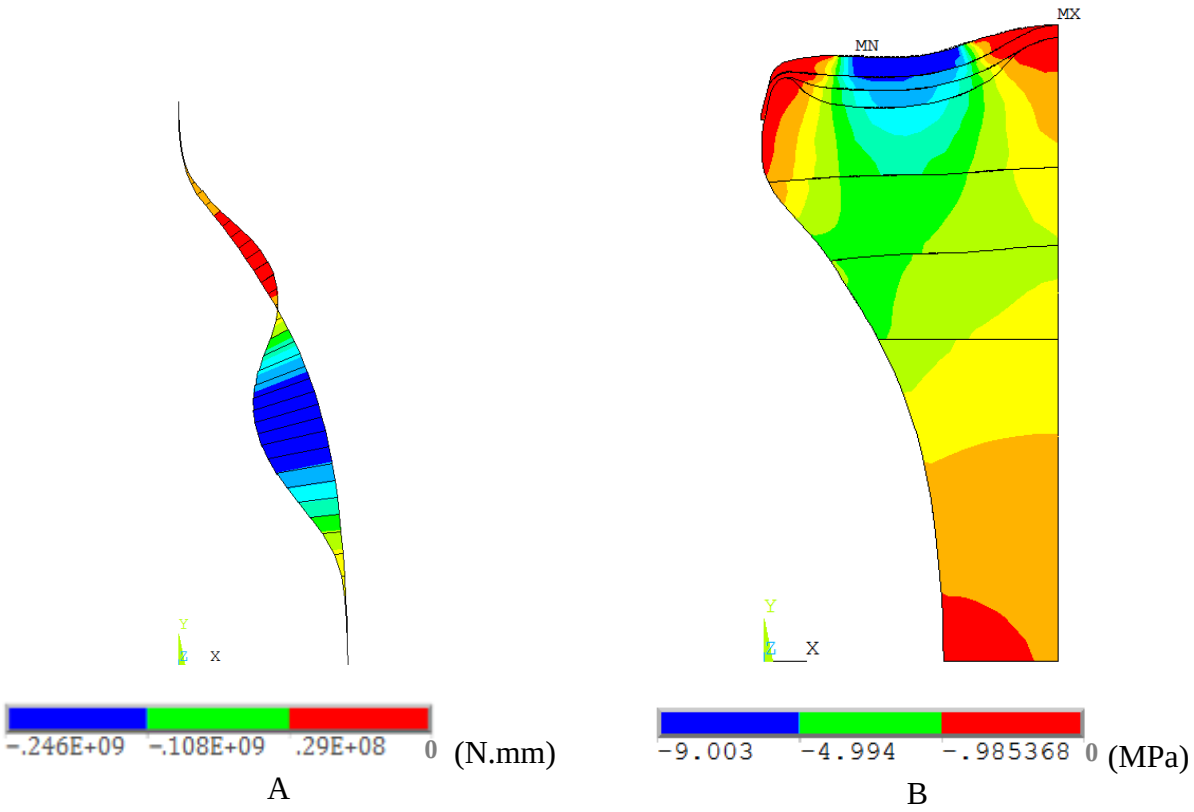

Figure 7-3) A. The bending moment graph along the cortical diaphysis of the proximal tibia. The more proximal section shown in red is bearing clockwise bending moment as in the distal blue region counter clockwise bending moment is shown. B. The principal compressive stress (S3) contour plot in the cartilage, proximal cortical and all trabecular regions. The stress flow from the articulating surface through the cartilage and subchondral bone to the cortical diaphysis is clearly shown. These two graphs together can give us valuable information regarding the load transfer mechanism in the knee joint.

Based on our preliminary results, the curved geometry and compressive loading condition of the proximal tibia leads to a clockwise bending moment in the proximal section of the peripheral cortical bone (shown by red in Figure 7-3 A). However, as shown in Figure 7-3 B, the

compressive load is transferred to the cortical diaphysis mostly at the curvature turning section of the bone, resulting in large values of counter-clockwise bending moment in the cortical diaphysis distal to this region. The rotation of different parts of the cortical bone relative to each other is shown in Figure 7-4. It also can be seen that a minimum amount of load goes through the subchondral periphery of the bone, where the osteophyte formation is mostly observed in OA conditions (Figure 7-3 B). The importance of understanding the load transmission mechanism comes from the fact that altering the morphology and/or stiffness of different layers of the subchondral bone might affect the normal load flow through these layers (e.g. deviate the compressive stress pattern towards the peripheral edge of the proximal tibia). These deviations, in turn, may increase the bone modeling/bone absorption process in different loaded/unloaded regions and result in osteophyte formation/local osteopenia.

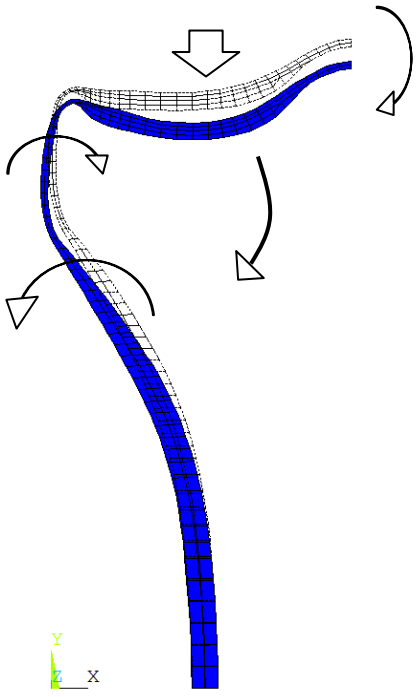

Figure 7-4) Subchondral cortical and cortical diaphysis of the proximal tibia deflected under pressure loading. The outline shows the initial geometry of the bone. The arrows are showing the rotation direction of different sections of the bone which are resulted from the bending moments exerted to these sections.

The preliminary results from the full knee model, described in the last section, also indicate a relationship between the loading profile on the cartilage and the load transmission pattern within the bone. The altered load profile in this model compared to the proximal tibial model resulted in a different compressive stress pattern (Figure 7-5). The altered load distribution, however, did not change relative effect of the parameters on overall stiffness of the proximal tibia (Table 7-1).

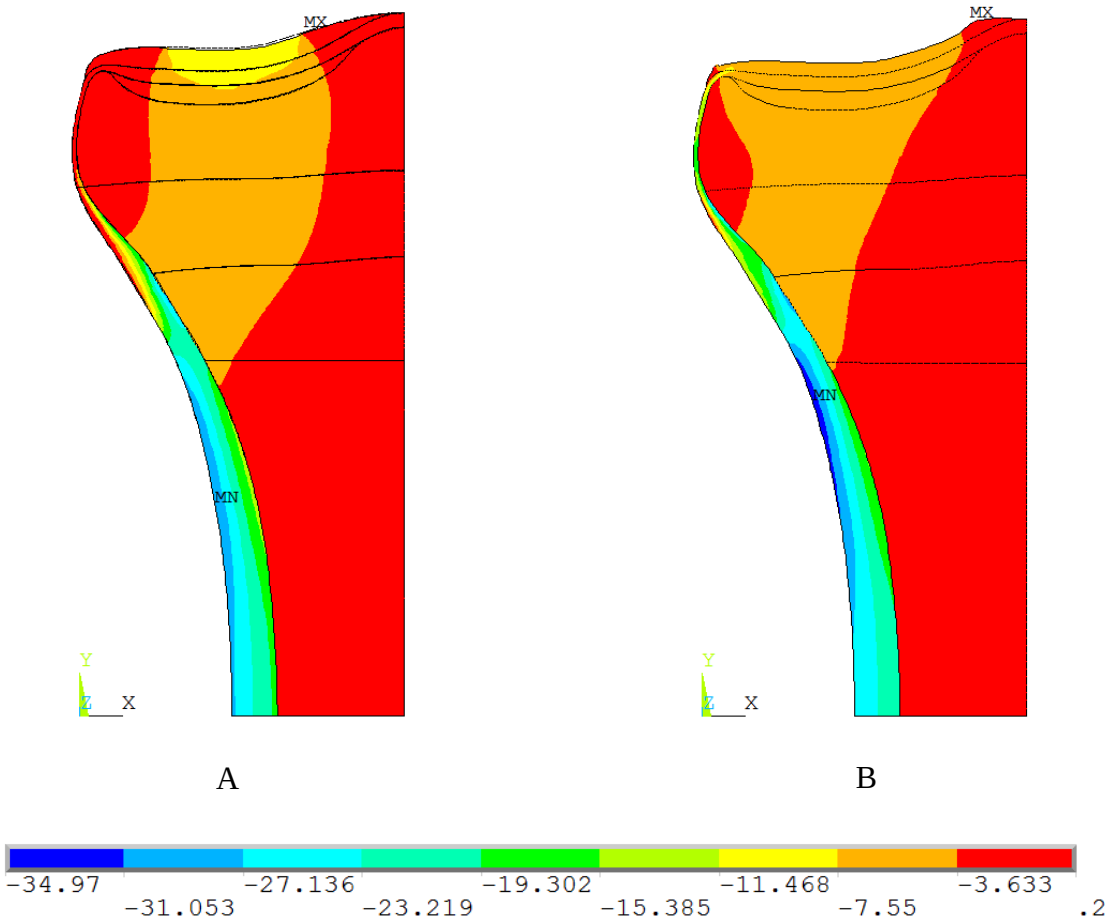

Figure 7-5) Principal compressive stress contour plot for A. original proximal tibial model with uniform loading and B. isolated proximal tibia from the full knee model in which the load is applied to the distal femur and transfers to the proximal tibia through femoral cartilage and meniscus. Different loading profiles have altered the stress distribution inside the bone.

Table 7-1) The combined effect of altering parameters on the overall stiffness of the proximal tibia for proximal tibial model and full knee model. The improved loading condition had little effect on overall stiffness of the bone. K/K_{norm} for each model has been calculated using its own K_{norm} value.

-20%	Normal	+20%	K/K_{norm}	
			Proximal Tibial Model	**Full Knee Model**
	ETS	SCT, SCS, STT, STS	1.019	1.015
ETS	SCT, SCS, STT, STS		0.898	0.903

To further improve our understanding of the load transmission mechanism and structural role of each different layer of subchondral bone on the stress distribution within the bone and cartilage, in addition to the suggested method in previous section for the full knee model modifications, more accurate material properties covering the complicated material behavior of different tissues of the proximal tibia appears necessary. Accordingly, different material modeling assumptions and related suggested improvements are discussed in the next section.

7.4.2 Material models

The trabecular bone in the subchondral and epiphyseal layers of the proximal tibia have heterogeneous material properties [81] which have been simplified by homogeneous assumptions in the current model. For further improvements in determination of relative effects of mechanical and morphologic properties of different cortical and trabecular layers in the proximal tibia, non-homogeneous material properties for the subchondral and epiphyseal trabecular layers could be included in the model.

Anisotropic material properties in the subchondral trabecular and epiphyseal trabecular bone, due to varying trabecular orientation in these regions [55], would also affect the stress distribution within the bone and might also influence the relative role of different parameters on the overall stiffness of the bone. These layers could be modeled with orthotropic material properties reported in the literature which would increase the accuracy of the FEM results regarding effects of epiphyseal trabecular bone on the overall stiffness of the bone, and ultimately the cartilage layer.

7.4.3 Cartilage modeling

In order to study the correlation between the bony alterations and the cartilage degeneration, effects of altering mechanical and morphologic properties alterations on the cartilaginous stresses should be identified. The poroelastic composite structure of the cartilage, with collagen fibers and proteoglycan media, can be modeled with different degrees of complexity and simplifications. The fibril orientation of the composite structure in the cartilage varies with the depth of cartilage from articulating surface parallel with the surface, random orientation in deeper sections and perpendicular to bone at the cartilage-bone boundary (Figure 7-6). In this study, as the outcomes (overall stiffness and stress distributions) were related to the bone, elastic-homogeneous-isotropic material properties were assigned to the cartilage layer. There are a variety of more complex models currently employed in biomechanical research [82, 83], most notably the layered isotropic model and the transversely isotropic model. The layered isotropic model does take into account the effect of different fibril orientation inside the cartilage. It assumes cartilage as a multilayered material with different isotropic material properties for each layer. This is important because the stress distribution within the cartilage layer may vary based on different fibril orientation and resultant stiffness inside the cartilage, which our current

cartilage FE model does not incorporate. The transversely isotropic model improves the model used in this study further more. This model also includes the anisotropy that exists within each layer of the cartilage. This is important because this would result in even more accurate stress distribution results compared to isotropic and layered isotropic models [82]. Future research building upon these thesis findings would benefit from incorporation of either of these cartilage models.

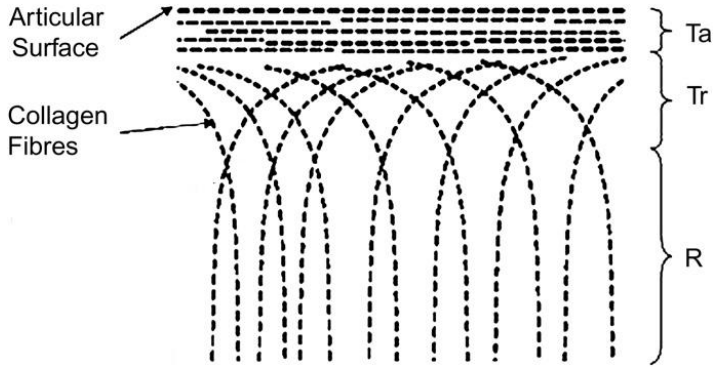

Figure 7-6) A schematic plot of the fibril orientation in different depth of the cartilage. Different layers are labeled as Ta: tangential, Tr: translational and R: radial. Modified from Bell et al [82] with permission from Elsevier.

7.4.4 Geometry of the bone

The geometry of proximal tibial bone and thickness of different subchondral bone layers might differ from subject to subject which may influence effect of different mechanical and morphological parameters on the overall stiffness of the bone. More importantly, the stress distribution within the bone and cartilage layers, as discussed in load transmission section, is correlated with the geometry of the bone and load distribution on the cartilage (which itself is also dependant on the distal tibial geometry). Using CT images of different proximal tibial samples, a segmentation MATLAB code has been developed to be used in building FE models with subject specific geometry (Figure 7-7).

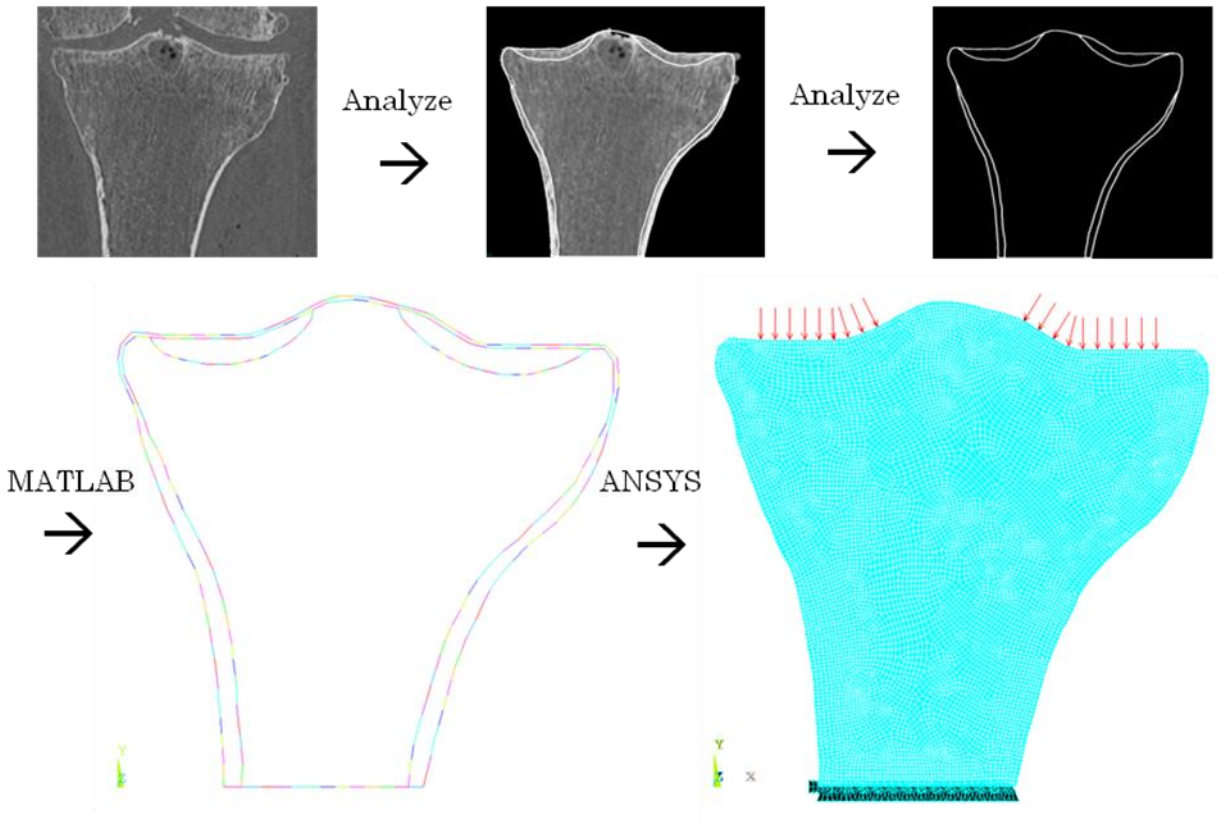

Figure 7-7) Process of generating a FE model out of a QCT image of the bone using ANALYZE for initial segmentation and boundary definition, and MATLAB for segmenting different layers and importing the coordinates to ANSYS for FE analysis.

7.4.5 3D modeling

Subject specific 3D FE models based on QCT/MRI images are very effective tools in order to account for inter subject differences in terms of overall geometry of the bone and morphological and mechanical properties of different subchondral bone layers. These models also eliminate the errors related to 2D modeling, such as oversimplified geometry, simplified material properties distribution, and generic morphology of different subchondral bone layers. Also, the non-invasive nature of this method enables researchers to conduct longitudinal studies on patients to monitor the mechanical alterations in their bones during OA progression and obtain deeper understanding of the structural role of subchondral bone in OA pathogenesis. This

work is currently being conducted at the university of Saskatchewan (JD Johnston and SM Nazemi) using QCT images of proximal tibial samples and ABAQUS. Moreover, to impose subject-specific boundary conditions to the 3D FE model of the bone, and also apply more realistic loading conditions compared to static loadings, flexible multibody dynamics approach can be used [84].

References

1. Kwan Tat, S., et al., *Targeting subchondral bone for treating osteoarthritis: what is the evidence?* Best Practice & Research Clinical Rheumatology, 2010. **24**(1): p. 51-70.
2. Johnston, J.D., B.A. Masri, and D.R. Wilson, *Computed tomography topographic mapping of subchondral density (CT-TOMASD) in osteoarthritic and normal knees: methodological development and preliminary findings.* Osteoarthritis and Cartilage, 2009. **17**(10): p. 1319-1326.
3. Canada, S. *Statistics Canada.* 2010; Available from: www.statcan.gc.ca.
4. Bobinac, D., et al., *Changes in articular cartilage and subchondral bone histomorphometry in osteoarthritic knee joints in humans.* Bone, 2003. **32**(3): p. 284-90.
5. Boyd, S.K., et al., *Early regional adaptation of periarticular bone mineral density after anterior cruciate ligament injury.* J Appl Physiol, 2000. **89**(6): p. 2359-64.
6. Li, B. and R.M. Aspden, *Material properties of bone from the femoral neck and calcar femorale of patients with osteoporosis or osteoarthritis.* Osteoporos Int, 1997. **7**(5): p. 450-6.
7. Li, B. and R.M. Aspden, *Composition and Mechanical Properties of Cancellous Bone from the Femoral Head of Patients with Osteoporosis or Osteoarthritis.* Journal of Bone and Mineral Research, 1997. **12**(4): p. 641-651.
8. Li, B. and R.M. Aspden, *Mechanical and material properties of the subchondral bone plate from the femoral head of patients with osteoarthritis or osteoporosis.* Ann Rheum Dis, 1997. **56(4)**: p. 247-54.
9. Kamibayashi, L., et al., *Trabecular microstructure in the medial condyle of the proximal tibia of patients with knee osteoarthritis.* Bone, 1995. **17**(1): p. 27-35.
10. Radin, E.L. and R.M. Rose, *Role of subchondral bone in the initiation and progression of cartilage damage.* Clin Orthop Relat Res, 1986(213): p. 34-40.
11. Burr, D.B. and E.L. Radin, *Microfractures and microcracks in subchondral bone: are they relevant to osteoarthrosis?* Rheumatic Disease Clinics of North America, 2003. **29**(4): p. 675-685.
12. Bennell, K.L., et al., *Tibial subchondral trabecular volumetric bone density in medial knee joint osteoarthritis using peripheral quantitative computed tomography technology.* Arthritis & Rheumatism, 2008. **58**(9): p. 2776-2785.
13. Johnston, J.D., et al., *Predicting subchondral bone stiffness using a depth-specific QCT topographic mapping technique in normal and osteoarthritic proximal tibiae.* Clin Biomech (Bristol, Avon), 2011.
14. Buckland-Wright, C., *Subchondral bone changes in hand and knee osteoarthritis detected by radiography.* Osteoarthritis and Cartilage, 2004. **12, Supplement**(0): p. 10-19.
15. Brandt, K.D., et al., *Osteoarthritic changes in canine articular cartilage, subchondral bone, and synovium fifty-four months after transection of the anterior cruciate ligament.* Arthritis Rheum, 1991. **34**(12): p. 1560-70.

16. Messent, E.A., J.C. Buckland-Wright, and G.M. Blake, *Fractal analysis of trabecular bone in knee osteoarthritis (OA) is a more sensitive marker of disease status than bone mineral density (BMD).* Calcif Tissue Int, 2005. **76**(6): p. 419-25.
17. Messent, E.A., et al., *Cancellous bone differences between knees with early, definite and advanced joint space loss; a comparative quantitative macroradiographic study.* Osteoarthritis Cartilage, 2005. **13**(1): p. 39-47.
18. Messent, E.A., et al., *Differences in trabecular structure between knees with and without osteoarthritis quantified by macro and standard radiography, respectively.* Osteoarthritis Cartilage, 2006. **14**(12): p. 1302-5.
19. Dedrick, D.K., et al., *A longitudinal study of subchondral plate and trabecular bone in cruciate-deficient dogs with osteoarthritis followed up for 54 months.* Arthritis Rheum, 1993. **36**(10): p. 1460-7.
20. Messent, E.A., et al., *Osteophytes, juxta-articular radiolucencies and cancellous bone changes in the proximal tibia of patients with knee osteoarthritis.* Osteoarthritis Cartilage, 2007. **15**(2): p. 179-86.
21. van der Kraan, P.M. and W.B. van den Berg, *Osteophytes: relevance and biology.* Osteoarthritis and Cartilage, 2007. **15**(3): p. 237-244.
22. Hayes, W.C., L.W. Swenson Jr, and D.J. Schurman, *Axisymmetric finite element analysis of the lateral tibial plateau.* Journal of biomechanics, 1978. **11**(1–2): p. 21-33.
23. Dar, F.H. and R.M. Aspden, *A finite element model of an idealized diarthrodial joint to investigate the effects of variation in the mechanical properties of the tissue.* Journal of Engineering in Medicine, 2003(217): p. 341-348.
24. Little, R.B., et al., *A three-dimensional finite element analysis of the upper tibia.* Journal of Biomechanical Engineering, 1986. **108**: p. 111-119.
25. Brown, T.D., et al., *Finite element studies of some juxtarticular stress changes due to localized subchondral stiffening.* Journal of biomechanics, 1984. **17**(1): p. 11-24.
26. Schipplein, O.D. and T.P. Andriacchi, *Interaction between active and passive knee stabilizers during level walking.* J Orthop Res, 1991. **9**(1): p. 113-9.
27. Mow, V.C., W.Y. Gu, and F.H. Chen, *Structure and function of articular cartilage and meniscus*, in *Basic Orthopaedic Biomechanics and Mechano-Biology*, V.C. Mow and R. Huiskes, Editors. 2005, Lippincott Williams and Wilkins: Philadelphia. p. 182-258.
28. Williams, P.L., et al., *Gray's Anatomy*. 37 ed, ed. P.L. Williams, et al.1989, London: Churchill Livingstone.
29. Seedhom, B.B., D. Dowson, and V. Wright, *Proceedings: Functions of the menisci. A preliminary study.* Ann Rheum Dis, 1974. **33**(1): p. 111.
30. Kurosawa, H., T. Fukubayashi, and H. Nakajima, *Load-bearing mode of the knee joint: physical behavior of the knee joint with or without menisci.* Clin Orthop Relat Res, 1980(149): p. 283-90.
31. Walker, P.S. and M.J. Erkman, *The role of the menisci in force transmission across the knee.* Clin Orthop Relat Res, 1975(109): p. 184-92.
32. Radin, E.L. and I.L. Paul, *Importance of bone in sparing articular cartilage from impact.* Clin Orthop Relat Res, 1971. **78**: p. 342-4.
33. *Geistlich Surgery*. 2012; Available from: http://www.geistlich-surgery.com.

34. Brandt, K.D., P. Dieppe, and E.L. Radin, *Etiopathogenesis of osteoarthritis.* Rheum Dis Clin North Am, 2008. **34**(3): p. 531-59.
35. Brandt, K.D., H.J. Mankin, and L.E. Shulman, *Workshop on etiopathogenesis of osteoarthritis.* J Rheumatol, 1986. **13**: p. 35.
36. Li, B. and R.M. Aspden, *Mechanical and material properties of the subchondral bone plate from the femoral head of patients with osteoarthritis or osteoporosis.* Ann Rheum Dis, 1997. **56**(4): p. 247-54.
37. Li, B. and R.M. Aspden, *Composition and mechanical properties of cancellous bone from the femoral head of patients with osteoporosis or osteoarthritis.* J Bone Miner Res, 1997. **12**(4): p. 641-51.
38. Zysset, P.K., M. Sonny, and W.C. Hayes, *Morphology-mechanical property relations in trabecular bone of the osteoarthritic proximal tibia.* J Arthroplasty, 1994. **9**(2): p. 203-16.
39. Lereim, P., I. Goldie, and E. Dahlberg, *Hardness of the subchondral bone of the tibial condyles in the normal state and in osteoarthritis and rheumatoid arthritis.* Acta Orthop Scand, 1974. **45**(4): p. 614-27.
40. Day, J.S., et al., *A decreased subchondral trabecular bone tissue elastic modulus is associated with pre-arthritic cartilage damage.* J Orthop Res, 2001. **19**(5): p. 914-8.
41. Ding, M., et al., *Changes in the stiffness of the human tibial cartilage-bone complex in early-stage osteoarthrosis.* Acta Orthop Scand, 1998. **69**(4): p. 358-62.
42. Ding, M., C.C. Danielsen, and I. Hvid, *Bone density does not reflect mechanical properties in early-stage arthrosis.* Acta Orthop Scand, 2001. **72**(2): p. 181-5.
43. Finlay, J.B., et al., *Stiffness of bone underlying the tibial plateaus of osteoarthritic and normal knees.* Clinical Orthopaedics and Related Research, 1989. **247**: p. 193-201.
44. Aigner, T. and L. McKenna, *Molecular pathology and pathobiology of osteoarthritic cartilage.* Cell Mol Life Sci, 2002. **59**(1): p. 5-18.
45. Karvonen, R.L., et al., *Periarticular osteoporosis in osteoarthritis of the knee.* J Rheumatol, 1998. **25**(11): p. 2187-94.
46. Grynpas, M.D., et al., *Subchondral bone in osteoarthritis.* Calcif Tissue Int, 1991. **49**(1): p. 20-6.
47. Buckland-Wright, C., *Subchondral bone changes in hand and knee osteoarthritis detected by radiography.* Osteoarthritis Cartilage, 2004. **12 Suppl A**: p. S10-9.
48. Cox, L.G.E., et al., *Decreased bone tissue mineralization can partly explain subchondral sclerosis observed in osteoarthritis.* Bone, 2012. **50**(5): p. 1152-1161.
49. Chappard, C., et al., *Subchondral bone micro-architectural alterations in osteoarthritis: a synchrotron micro-computed tomography study.* Osteoarthritis Cartilage, 2006. **14**(3): p. 215-23.
50. Ding, M., A. Odgaard, and I. Hvid, *Changes in the three-dimensional microstructure of human tibial cancellous bone in early osteoarthritis.* Bone & Joint Surgery, 2003. **85-B**: p. 906-12.
51. Clark, J.M. and J.D. Huber, *The structure of the human subchondral plate.* J Bone Joint Surg Br, 1990. **72**(5): p. 866-73.
52. Milz, S. and R. Putz, *Quantitative morphology of the subchondral plate of the tibial plateau.* J Anat, 1994. **185 (Pt 1)**: p. 103-10.

53. Yamada, K., et al., *Subchondral bone of the human knee joint in aging and osteoarthritis.* Osteoarthritis Cartilage, 2002. **10**(5): p. 360-9.
54. Matsui, H., M. Shimizu, and H. Tsuji, *Cartilage and subchondral bone interaction in osteoarthrosis of human knee joint: a histological and histomorphometric study.* Microsc Res Tech, 1997. **37**(4): p. 333-42.
55. Kamibayashi, L., et al., *Trabecular microstructure in the medial condyle of the proximal tibia of patients with knee osteoarthritis.* Bone, 1995. **17**(1): p. 27-35.
56. Chiba, K., et al., *Relationship between microstructure and degree of mineralization in subchondral bone of osteoarthritis: A synchrotron radiation μCT study.* Journal of Bone and Mineral Research, 2012. **27**(7): p. 1511-1517.
57. Li, B., et al., *The electron microscope appearance of the subchondral bone plate in the human femoral head in osteoarthritis and osteoporosis.* J Anat, 1999. **195 (Pt 1)**: p. 101-10.
58. Mansell, J.P. and A.J. Bailey, *Abnormal cancellous bone collagen metabolism in osteoarthritis.* J Clin Invest, 1998. **101**(8): p. 1596-603.
59. Johnston, J.D., B.A. Masri, and D.R. Wilson, *Computed tomography topographic mapping of subchondral density (CT-TOMASD) in osteoarthritic and normal knees: methodological development and preliminary findings.* Osteoarthritis Cartilage, 2009. **17**(10): p. 1319-26.
60. Brown, T.D., et al., *Finite element studies of some juxtarticular stress changes due to localized subchondral stiffening.* J Biomech, 1984. **17**(1): p. 11-24.
61. Little, R.B., et al., *A three-dimensional finite element analysis of the upper tibia.* J Biomech Eng, 1986. **108**(2): p. 111-9.
62. Brandt, K.D., P. Dieppe, and E.L. Radin, *Etiopathogenesis of Osteoarthritis.* Rheumatic Disease Clinics of North America, 2008. **34**(3): p. 531-559.
63. Zysset, P.K., M. Sonny, and W.C. Hayes, *Morphology-mechanical property relations in trabecular bone of the osteoarthritic proximal tibia.* The Journal of Arthroplasty, 1994. **9**(2): p. 203-216.
64. Lereim, P., I. Goldie, and E. Dahlberg, *Hardness of the Subchondral Bone of the Tibial Condyles in the Normal State and in Osteoarthritis and Rheumatoid Arthritis.* Acta Orthopaedica, 1974. **45**(1-4): p. 614-627.
65. Day, J.S., et al., *A decreased subchondral trabecular bone tissue elastic modulus is associated with pre-arthritic cartilage damage.* Journal of Orthopaedic Research, 2001. **19**(5): p. 914-918.
66. Ding, M., et al., *Changes in the stiffness of the human tibial cartilage-bone complex in early-stage osteoarthrosis.* Acta Orthopaedica, 1998. **69**(4): p. 358-362.
67. Ding, M., C.C. Danielsen, and I. Hvid, *Bone density does not reflect mechanical properties in early-stage arthrosis.* Acta Orthop Scand, 2001. **72(2)**: p. 181-185.
68. Keyak, J.H., *Improved prediction of proximal femoral fracture load using nonlinear finite element models.* Medical Engineering & Physics, 2001. **23**(3): p. 165-173.
69. Choi, K., et al., *The elastic moduli of human subchondral, trabecular, and cortical bone tissue and the size-dependency of cortical bone modulus.* J Biomech, 1990. **23**(11): p. 1103-13.

70. Bentzen, S.M., I. Hvid, and J. Jorgensen, *Mechanical strength of tibial trabecular bone evaluated by X-ray computed tomography.* J Biomech, 1987. **20**(8): p. 743-52.
71. Morgan, E.F., H.H. Bayraktar, and T.M. Keaveny, *Trabecular bone modulus-density relationships depend on anatomic site.* J Biomech, 2003. **36**(7): p. 897-904.
72. Buckland-Wright, J.C., J.A. Lynch, and B. Dave, *Early radiographic features in patients with anterior cruciate ligament rupture.* Ann Rheum Dis, 2000. **59**(8): p. 641-6.
73. Keyak, J.H., I.Y. Lee, and H.B. Skinner, *Correlations between orthogonal mechanical properties and density of trabecular bone: use of different densitometric measures.* Journal of biomedical materials research, 1994. **28**(11): p. 1329-36.
74. Hohe, J., et al., *Surface size, curvature analysis, and assessment of knee joint incongruity with MRI in vivo.* Magnetic Resonance in Medicine, 2002. **47**(3): p. 554-561.
75. Helgason, B., et al., *Mathematical relationships between bone density and mechanical properties: A literature review.* Clinical Biomechanics, 2008. **23**(2): p. 135-146.
76. Johnston, J.D., et al., *In Vivo Precision of Computed Tomography Topographic Mapping of Subchondral Density (CT-TOMASD) in the Proximal Tibia.* Transactions of the 34nd Orthopaedic Research Society Meeting, 2009(242).
77. Messent, E.A., et al., *Osteophytes, juxta-articular radiolucencies and cancellous bone changes in the proximal tibia of patients with knee osteoarthritis.* Osteoarthritis and Cartilage, 2007. **15**(2): p. 179-186.
78. Pugh, J.W., R.M. Rose, and E.L. Radin, *Elastic and viscoelastic properties of trabecular bone: Dependence on structure.* Journal of biomechanics, 1973. **6**(5): p. 475-485.
79. Huiskes, R., J.D. Janssen, and T.J. Slooff. *A Detailed Comparison of Experimental and Theoretical Stress-Analyses of a Human Femur*. in *ASME-ASCE Applied mehanica, Fluid Engineering and Bioengineering Conference*. 1981.
80. Meakin, J.R., et al., *Finite element analysis of the meniscus: the influence of geometry and material properties on its behaviour.* The Knee, 2003. **10**(1): p. 33-41.
81. Harada, Y., H.W. Wevers, and T.D. Cooke, *Distribution of bone strength in the proximal tibia.* J Arthroplasty, 1988. **3**(2): p. 167-75.
82. Bell, J.S., et al., *Modeling the steady-state deformation of the solid phase of articular cartilage.* Biomaterials, 2009. **30**(31): p. 6394-6401.
83. Mononen, M., et al., *Alterations in structure and properties of collagen network of osteoarthritic and repaired cartilage modify knee joint stresses.* Biomechanics and Modeling in Mechanobiology, 2011. **10**(3): p. 357-369.
84. Al Nazer, R., et al., *Flexible multibody simulation approach in the analysis of tibial strain during walking.* Journal of biomechanics, 2008. **41**(5): p. 1036-1043.

8 Appendix

8.1 Theoretical background

In this section a brief description of the assumptions and options used in different FE modeling studies (including my FE analysis) is provided:

8.1.1 Material models

8.1.1.1 Linear elastic materials

If a load or deformation is applied to a solid material an internal stress distribution is created in it. A material is defined as an *elastic* material when the structure made of this material returns exactly to its original shape after removing the applied load on it. This behavior can be found in almost all engineering materials in cases where the external loads are not too large. Typically, with modeling we assume small deformations in our problems so that the material can be considered *linearly* elastic, which means the stress and strain (σ and ε) are related to each other with a *linear* equation:

$$\begin{Bmatrix}\sigma_x\\ \sigma_y\\ \tau_{xy}\end{Bmatrix} = \frac{E}{(1+\upsilon)(1-2\upsilon)}\begin{bmatrix}1-\upsilon & \upsilon & 0\\ \upsilon & 1-\upsilon & 0\\ 0 & 0 & \frac{1-\upsilon}{2}\end{bmatrix}\begin{Bmatrix}\varepsilon_x\\ \varepsilon_y\\ \gamma_{xy}\end{Bmatrix}$$

in which the coefficient "E" is called "Young's modulus of elasticity" which indicates the *material stiffness* and υ is the "Poisson's ratio".

8.1.1.2 Isotropic and homogeneous material properties

We assume a material body to be *homogeneous* if the matter is continuously distributed over it, in a way that the smallest part of the homogenous body possesses identical physical properties

compared to the whole body. Also if the mechanical properties of a material (e.g. material stiffness) are the same in all directions, that material is called an *isotropic* material. This differs from *anisotropic* materials with different mechanical properties in different directions, like wood.

8.1.2 Two-Dimensional Elasticity

Two general types of problems exist in 2D (plane theory of elasticity) analyses which are *plane stress* and *plane strain.* Many sophisticated problems in elasticity domain can be modeled using these two methods with sufficient accuracy. These methods are applicable to the problems using some definite assumptions and simplifications which will be illustrated here.

8.1.2.1 Plane Stress

In this type of problems the normal stress perpendicular to a plane (say the x-y plane), σ_z, and the σ_{xz} and σ_{yz} shear stresses are assumed to be zero. For a structure to fall into this category of the plane elasticity problems the geometry should be similar to plate with a thickness much smaller relative to the other two dimensions. Also, the loading condition in this case would be uniform loading applied to the thickness of the plate and acting in the plane of the plate (as in the figure bellow the load is shown by T) (Figure 8-1).

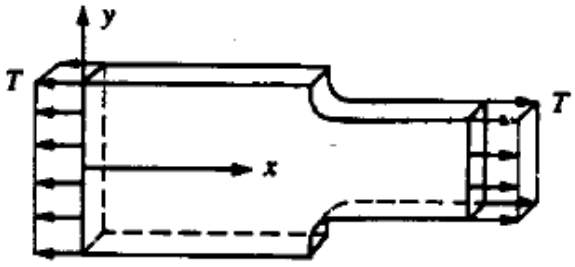

Figure 8-1) A thin plate with fillets. The thickness is relatively smaller than other two dimensions of the plate which enables us to use plane stress assumptions to analyze it.

8.1.2.2 Plane Strain

In the *plane strain* type of 2D elasticity problems the strain normal to the x-y plane, ε_z, should be zero as well as the shear strains γ_{xz} and γ_{yz}. The conditions for which this state of strain is applicable occur when one dimension of the structure (z axis) is much larger relative to the other two dimensions (x,y). The forces in this scenario also act in the plane formed by the smaller two dimensions (x-y plane) and do not vary along the third axis. An example of this kind of problems would be analysis of dams, or retaining (Figure 8-2).

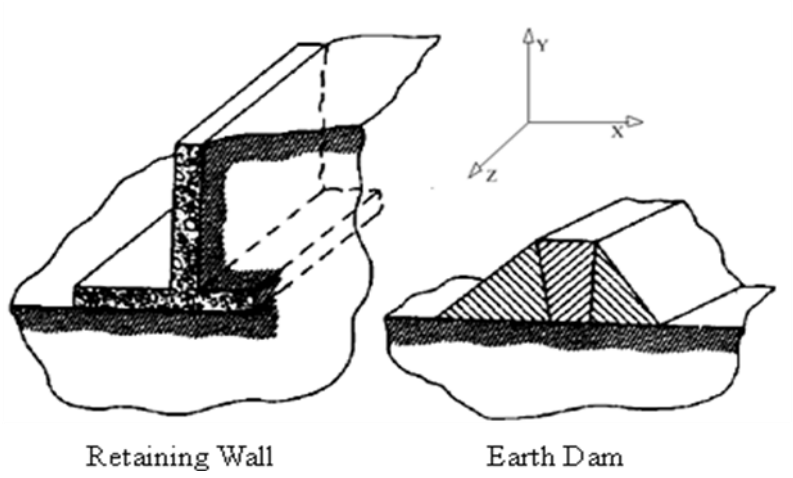

Figure 8-2) Two samples of engineering structures with a relatively large dimension (z) compared to their other two dimensions (x,y). These structures can be analyzed using plane strain assumptions.

8.1.2.3 Axisymmetric

Another class of 2D modeling approaches is axisymmetric modeling. For a structure to qualify for this analysis, a rotationally symmetric geometry is necessary. But this condition does not necessarily result in the problem to be defined as an axisymmetric problem. The other essential

condition would be that the loading and the boundary condition also be rotationally symmetric. Examples of such structure are pipes, pressurized tanks and rockets in aerospace industry.

8.1.2.4 Element selection

PLANE42 element type is used for the 2D modeling of the proximal tibial model. This element is capable of being used as a plane element (plane stress or plane strain) or as an axisymmetric element. In our modeling all three types have been used to compare the results and select the most appropriate modeling approach. This element can be defined by four nodes with two degrees of freedom: translations in the nodal x and y directions, at each node. Strain and stress results from the large variety of output options for this element have been used in our analysis.

As the PLANE42 element cannot provide the bending moments and shear forces, BEAM3 uniaxial elastic element was used to get the bending moment distribution in the peripheral and diaphyseal cortical bone. This element has three degrees of freedom at each node: translations in the nodal x and y directions and rotation about the nodal z axis.

8.2 Proximal tibial FE modeling ANSYS code

```
! Initializing
Finish
/clear
/prep7
/title,Tibia1


!-----------------------Parameters-----------------------------
sc=2.6   !Pixel to millimeter conversion factor
sf=1     !Mesh size factor. Larger numbers refine the mesh (tested up to sf=5)

!t1: Subchondral cortical thickness (mm)
!t2: subchondral Trabecular thickness (mm)
!t3: cortical wall starting thickness (mm)(cortical diaphysis thickness is varying along the bone)
!t4: Cartilage thickness (mm)
!t5: Epiphysial thickness (mm)

!E1: Subchondral cortical E (MPa)
!E2: Subchondral Trabecular E (MPa)
!E3: Cortical wall E MPa
!E4: Cartilage E (MPa)
!E5: epiphysial Trabecular E (MPa)
!E6: metaphysial Trabecular E (MPa)

! Typical values representing normal proxinal tibia
!t1=2
!t2=t1+2.5
!t3=1
!t4=3
!t5=15

!E1=2000
!E2=500
!E3=14000
!E4=15
!E5=500
!E6=300

t1=1.2
t2=t1+2.5
t3=1
t4=3
t5=15

E4=15

E1=1000
Npcor=E1/E4      !Relative stiffness of the subchondral cortical bone with respect to Cartilage

E2=500
NSub=E2/E4       !Relative stiffness of the subchondral trabecular bone with respect to Cartilage

E3=14000
```

```
Ncorw=E3/E4     !Relative stiffness of the cortical wall with respect to Cartilage

E5=300
Netra=E5/E4     !Relative stiffness of the epiphyseal trabecular bone with respect to Cartilage

E6=300
Nmtra=E6/E4     !Relative stiffness of the metaphyseal trabecular bone with respect to Cartilage

!------------------------Material Properties-------------------

!Poisson's ratios from literature

!mat 1(Subchondral cortical)
Mp,ex,1,E1
Mp,prxy,1,.3

!Mat 2(subchondral trabecular)
Mp,ex,2,E2
Mp,prxy,2,.3

!mat 3(cortical Wall)
Mp,ex,3,E3
Mp,prxy,3,.3

!mat 4(cartilage)
Mp,ex,4,E4
Mp,prxy,4,.4

!mat 5(epiphyseal trabecular)
Mp,ex,5,E5
Mp,prxy,5,.3

!mat 6(metaphyseal trabecular)
Mp,ex,6,E6
Mp,prxy,6,.3

!mat 7(metaphyseal trabecular 2) to have a coherent stiffness distribution
Mp,ex,7,E6+(E5-E6)*2/3
Mp,prxy,7,.3

!mat 8(metaphyseal trabecular 3) to have a coherent stiffness distribution
Mp,ex,8,E6+(E5-E6)/3
Mp,prxy,8,.3

!Setting element options
Et,1,plane42
KEYOPT,1,3,2    !for Plane strain analysis
!KEYOPT,1,3,1   !for Axisymmetric analysis
!KEYOPT,1,3,0   !for Plane stress analysis
Type,1

!------------------------Keypoints------------------------------
!Keypoint coordinates have been extracted from CT image of a proximal tibial sample.
!------------------------OutCort
!Outer boundary of the cortical bone (including subchondral cortical and cortical wall)
```

```
k,      1       ,       44.23   ,       96.15
k,      2       ,       37.50   ,       93.85
k,      3       ,       31.73   ,       90.77
k,      4       ,       23.08   ,       88.46
k,      5       ,       11.54   ,       88.46
k,      6       ,       5.77    ,       88.85
k,      7       ,       2.69    ,       88.85
k,      8       ,       0.58    ,       86.73

k,      40      ,       -0.38   ,       88.46-1.15-t5

k,      9       ,       6.5     ,       61.63-1.15
k,      10      ,       13.12   ,       48.65
k,      11      ,       17.50   ,       34.04
k,      12      ,       19.81   ,       19.42
k,      13      ,       20.77   ,       0
k,      14      ,       20.77+(6.2*t3)  ,       0
k,      15      ,       44.23   ,       0.00

k,      35      ,       44.23   ,       19.42
k,      36      ,       44.23   ,       34.04
k,      37      ,       44.23   ,       48.65
k,      38      ,       44.23   ,       61.63+1.15
k,      39      ,       44.23   ,       88.46+1.15-t5



!-------------------------Orientation vector parameters for splines
!These parameters are defined based on the next closest keypoint coordinates to ensure a smooth transition between two splines (each spline can go through a maximum number of 6 keypoints)

xv11=cos(0)             !xv11 denotes the vertical component of the starting slope for the first spline
yv11=cos(3.14/2)        !yv11 denotes the horizontal component of the starting slope for the first spline
xv61=-(30-15)/((30-15)**2+(231-230)**2)**0.5    !xv61 denotes the vertical component of the ending slope for
                                                !the first spline
yv61=(231-230)/((30-15)**2+(231-230)**2)**0.5

xv12=(60-30)/((60-30)**2+(230-230)**2)**0.5
yv12=(230-230)/((60-30)**2+(230-230)**2)**0.5
xv62=-(6.5-13.12)/((6.5-13.12)**2+(61.63-1.15-48.65)**2)**0.5
yv62=-(61.63-1.15-48.65)/((6.5-13.12)**2+(61.63-1.15-48.65)**2)**0.5

xv13=-(6.5-(-0.38))/((6.5-(-0.38))**2+((61.63-1.15)-(88.46-1.15-t5))**2)**0.5
yv13=-((61.63-1.15)-(88.46-1.15-t5))/((6.5-(-0.38))**2+((61.63-1.15)-(88.46-1.15-t5))**2)**0.5
xv63=cos(3.14/2)
yv63=-cos(0)


!-------------------------InCort
!Inner boundary of the cortical bone (including subchondral cortical and cortical wall)

k,      16,     44.23           ,       96.15-((1)*t1)
k,      17,     37.5+((0.7)*t1) ,       93.85-((0.7)*t1)
k,      18,     31.73+((0.5)*t1)  ,     90.77-((0.85)*t1)
k,      19,     23.08           ,       88.46-(t1)
k,      20,     11.54           ,       88.46-(t1)
```

```
k,      21,     5.77            ,       88.85-((0.7)*t1)
k,      22,     2.69+((0.2)*t1) ,       88.85-((0.35)*t1)
k,      23,     0.58+((0.5)*t1) ,       86.73-((0.5)*t1)

k,      41,     -0.38+(t1)      ,       88.46-1.15-(t5)

k,      24,     6.5+(3.5*t3)    ,       61.63-1.15

k,      26,     12.12+(5*t3)    ,       48.65
k,      27,     17.5+(5.5*t3)   ,       34.04
k,      28,     19.81+(6*t3)    ,       19.42


!-------------------------Orientation vector parameters for  splines
xv14=cos(0)
yv14=cos(3.14/2)
xv64=-(30-15)/((30-15)**2+(231-230)**2)**0.5
yv64=(231-230)/((30-15)**2+(231-230)**2)**0.5

xv15=(60-30)/((60-30)**2+(230-230)**2)**0.5
yv15=(230-230)/((60-30)**2+(230-230)**2)**0.5
xv65=-(6.5+(3.5*t3)-(12.12+(5*t3)))/((6.5+(3.5*t3)-(12.12+(5*t3)))**2+(61.63-1.15-48.65)**2)**0.5
yv65=-(61.63-1.15-48.65)/((6.5+(3.5*t3)-(12.12+(5*t3)))**2+(61.63-1.15-48.65)**2)**0.5

xv16=-(6.5+(3.5*t3)-(-0.38+(t1)))/((6.5+(3.5*t3)-(-0.38+(t1)))**2+(61.63-1.15-(88.46-1.15-(t5)))**2)**0.5
yv16=((230-t5)-180)/((4+(1.5*t3)-(-1+t1))**2+((230-t5)-180)**2)**0.5
xv66=cos(3.14/2)
yv66=-cos(0)

!-------------------------SubC
!Bottom boundary of the subchondral trabecular bone

k,      29,     31.73+(0.5*t2)  ,       90.77-(0.65*t2)
k,      30,     23.08   ,       88.46-t2
k,      31,     11.54   ,       88.46-t2
k,      44,     5.77    ,       88.85-0.6*t2

xv67=-cos(0)
yv67=cos(3.14/2)

!-------------------------Cartilage
!Upper boundary of the cartilage

k,      32,     31.73-(0.5*t4)  ,       90.77+(0.85*t4)
k,      33,     23.08   ,       88.46+t4
k,      34,     11.54   ,       88.46+t4
!k,     42,     5.77    ,       88.85+0.8*t4
k,      43,     2.69    ,       88.85+0.5*t4

xv18=cos(0)
yv18=cos(3.14/2)

!-------------------------Trabecular Midpoints
!Defined to curve the separating line between the epiphyseal, metaphyseal and diaphyseal trabecular regions

k,      45,     23.08   ,       88.46-t5
```

```
k,        46,       27.08    ,        61.63

!-------------------------Lines--------------------------------

!-----------------------OutCort

spline,1,2,3,4,5,,xv11,yv11,,xv61,yv61                !Line 1-4
spline,5,6,7,8,40,9,xv12,yv12,,xv62,yv62     !Line 5-9
spline,9,10,11,12,13,,xv13,yv13,,xv63,yv63 !Line 10-13

!-----------------------InCort
spline,16,17,18,19,20,,xv14,yv14,,xv64,yv64           !Line 14-17
spline,20,21,22,23,41,24,xv15,yv15,,xv65,yv65        !Line 18-22
spline,24,26,27,28,14,,xv16,yv16,,xv66,yv66           !Line 23-26


l,        13,       14                                !Line 27
l,        15,       14                                !Line 28
l,        15,       35                                !Line 29
l,        35,       28                                !Line 30
l,        35,       36                                !Line 31
l,        36,       27                                !Line 32
l,        36,       37                                !Line 33
l,        37,       26                                !Line 34
l,        37,       38                                !Line 35
spline,38,46,,,,,1,0,,-1,0                    !Line 36
l,        38,       39                                !Line 37
spline,39,45,,,,,1,0,,-1,0                    !Line 38
l,        39,       16                                !Line 39
l,        40,       41                                !Line 40

!-----------------------SubC
spline,17,29,30,31,44,22,0.8,0.5,,-0.98,-0.17 !Line 41-45
!spline,17,29,30,31,44,22                     !Line 41-45
l,        18,       29                                !Line 46
l,        19,       30                                !Line 47
l,        20,       31                                !Line 48
l,        21,       44                                !Line 49

!-------------------------Cartilage
spline,1,32,33,34,43,8,xv18,yv18              !Line 50-54
l,        3,        32                                !Line 55
l,        4,        33                                !Line 56
l,        5,        34                                !Line 57
l,        7,        43                                !Line 58

l,        1,        16                                !Line 59

spline,46,24,,,,,1,0                                  !Line 60
spline,45,41,,,,,1,0                                  !Line 61

!-------------------------Component Define-----------------------
!Lines grouped for convenient use in area definition and concatenation steps

lsel,s,line,,41,45
cm,SubCW,line                         !Subchondral region bottom line
```

```
lsel,s,line,,14
lsel,a,line,,20,21
lsel,a,line,,38,39
lsel,a,line,,61
cmsel,a,SubCW
cm,epi,line                    !Epiphyseal Trabecular

lsel,s,line,,1,8
lsel,a,line,,40
lsel,a,line,,59
lsel,a,line,,14,21
cm,PrCort,line                 !Proximal Cortical

lsel,s,line,,9,13
lsel,a,line,,22,27
lsel,a,line,,40
cm,Wcort,line                  !Cortical Wall

lsel,s,line,,50,54
lsel,a,line,,2,5
lsel,a,line,,40
lsel,a,line,,27
cm,Cart,line                   !Cartilage layer

lsel,s,line,,29
lsel,a,line,,31
lsel,a,line,,33
lsel,a,line,,35
lsel,a,line,,37
lsel,a,line,,39
lsel,a,line,,59
cm,sym,line                    !Symmetry Line

!-----------------------Areas--------------------------
!In this step areas are formed using the corresponding lines and the lines are meshed to achieve the most coherent
and mapped mesh possible
!sf (mesh size factor) as a mesh size controlling factor is multiplied to the line mesh numbers.

!-----------------------area 1 epi-Trabecular
cmsel,s,epi
al,all                         !Area     1
lesize,14,,,4*sf,,0,,,0
lesize,41,,,4*sf,,1,,,0
lesize,42,,,5*sf,,1,,,0
lesize,43,,,5*sf,,1,,,0
lesize,44,,,4*sf,,1,,,0
lesize,45,,,3*sf,,1,,,0
lesize,20,,,3*sf,,1,,,0
lesize,21,,,8*sf,,1,,,0
lesize,39,,,10*sf,0.6,1,,,0

!-----------------------areas 2-6 Meta-Trabecular
lsel,s,line,,36,38
lsel,a,line,,22
lsel,a,line,,60,61
```

```
al,all                          !Area    2
lesize,36,,,8*(sf),0.4,0,,,0
lesize,60,,,16*(sf),0.4,0,,,0
lesize,38,,,8*(sf),0.4,0,,,0
lesize,61,,,16*(sf),0.4,0,,,0
lesize,22,,,8*(sf),,0,,,0
lesize,37,,,8*(sf),,0,,,0

lsel,s,line,,34,36
lsel,a,line,,23
lsel,a,line,,60
al,all                          !Area    3
lesize,34,,,10*(sf),0.4,0,,,0
lesize,23,,,8*(sf),,0,,,0
lesize,35,,,8*(sf),,0,,,0

lsel,s,line,,32,34
lsel,a,line,,24
al,all                          !Area    4
lesize,32,,,10*(sf),0.4,0,,,0
lesize,24,,,8*(sf),,0,,,0
lesize,33,,,8*(sf),,0,,,0

lsel,s,line,,30,32
lsel,a,line,,25
al,all                          !Area    5
lesize,30,,,10*(sf),0.4,0,,,0
lesize,25,,,6*(sf),,0,,,0
lesize,31,,,6*(sf),,0,,,0

lsel,s,line,,28,30
lsel,a,line,,26
al,all                          !Area    6
lesize,28,,,10*(sf),0.4,0,,,0
lesize,26,,,6*(sf),,0,,,0
lesize,29,,,6*(sf),,0,,,0

!------------------------area 7-11 SubC
lsel,s,line,,41
lsel,a,line,,46
lsel,a,line,,15
al,all                          !Area    7
lesize,46,,,2*sf,,0,,,0
lesize,15,,,4*sf,,0,,,0

lsel,s,line,,42
lsel,a,line,,46,47
lsel,a,line,,16
al,all                          !Area    8
lesize,47,,,2*sf,,0,,,0
lesize,16,,,5*sf,,0,,,0

lsel,s,line,,43
lsel,a,line,,47,48
lsel,a,line,,17
al,all                          !Area    9
```

```
lesize,48,,,2*sf,,0,,,0
lesize,17,,,5*sf,,0,,,0

lsel,s,line,,44
lsel,a,line,,48,49
lsel,a,line,,18
al,all                                  !Area     10
lesize,49,,,2*sf,,0,,,0
lesize,18,,,4*sf,,0,,,0

lsel,s,line,,45
lsel,a,line,,49
lsel,a,line,,19
al,all                                  !Area     11
lesize,45,,,3*sf,,0,,,0
lesize,19,,,3*sf,,0,,,0

!------------------------area 12 Pr-Cortical
cmsel,s,PrCort
al,all
lesize,1,,,4*sf,,0,,,0
lesize,2,,,4*sf,,0,,,0
lesize,3,,,5*sf,,0,,,0
lesize,4,,,5*sf,,0,,,0
lesize,5,,,4*sf,,0,,,0
lesize,6,,,3*sf,,0,,,0
lesize,7,,,3*sf,,0,,,0
lesize,8,,,8*sf,,0,,,0

lesize,59,,,2*sf,,0,,,0
lesize,40,,,2*sf,,0,,,0

!------------------------area 13 Cortical-Wall
cmsel,s,WCort
al,all
lesize,9,,,8*(sf),,0,,,0
lesize,10,,,8*(sf),,0,,,0
lesize,11,,,8*(sf),,0,,,0
lesize,12,,,6*(sf),,0,,,0
lesize,13,,,6*(sf),,0,,,0
lesize,27,,,2*sf,,0,,,0

!------------------------area 14-18 Cartilage
lsel,s,line,,1,2
lsel,a,line,,55
lsel,a,line,,50
al,all                                  !Area     14
lesize,50,,,10*sf,,0,,,0
lesize,55,,,3*sf,,0,,,0

lsel,s,line,,3
lsel,a,line,,55,56
lsel,a,line,,51
al,all                                  !Area     15
lesize,51,,,5*sf,,0,,,0
lesize,56,,,3*sf,,0,,,0
```

```
lsel,s,line,,52
lsel,a,line,,56,57
lsel,a,line,,4
al,all                          !Area    16
lesize,52,,,5*sf,,0,,,0
lesize,57,,,3*sf,,0,,,0

lsel,s,line,,5,6
lsel,a,line,,57,58
lsel,a,line,,53
al,all                          !Area    17
lesize,53,,,7*sf,,0,,,0
lesize,58,,,3*sf,,0,,,0

lsel,s,line,,58
lsel,a,line,,7
lsel,a,line,,54
al,all                          !Area    18
lesize,54,,,3*sf,,0,,,0

!------------------------Concatenation
!Concatenating all the lines composing a single area which will have one material property in order to use mapped mesh option. Mapped mesh option is available only for areas comprised of 4 lines with the same element count on opposite lines.

lsel,s,line,,1,8
LCCAT,all
lsel,s,line,,14,21
LCCAT,all
lsel,s,line,,9,13
LCCAT,all
lsel,s,line,,22,26
LCCAT,all
lsel,s,line,,1,2
LCCAT,all
lsel,s,line,,5,6
LCCAT,all
lsel,s,line,,36
lsel,a,line,,60
LCCAT,all
lsel,s,line,,38
lsel,a,line,,61
LCCAT,all

cmsel,s,SubCW
lsel,a,line,,14
LCCAT,all

lsel,s,line,,20,21
LCCAT,all
!------------------------Meshing-------------------------
!Meshing the areas with PLANE42 elements. Mapped mesh is used where ever possible.

mshape,0,2D
```

```
mshkey,1
mat,1               !Subchondral Cortical
amesh,12

mshkey,1
mat,3               !Cortical Wall
amesh,13

mat,2               !Subchondral Trabecular
mshkey,2
amesh,7
amesh,11
mshkey,1
amesh,8,10

mat,4               !Cartilage
mshkey,0
amesh,14
amesh,18
mshkey,1
amesh,15,17

mshkey,0
mat,5               !epi. Trabecular
amesh,1

mshkey,1
mat,7               !meta. Trabecular
amesh,2

mshkey,0
mat,8
amesh,3

mshkey,1
mat,6
amesh,4,6

!-----------------------Constraints

nsel,s,loc,y,-1,0.1
D,all,UY,0                  !Fixing the most distal nodes in the vertical direction

nsel,s,loc,x,114.5/sc,115.5/sc
nsel,u,loc,y,0.1,500
D,all,all,0

!-----------------------Load
lsel,s,line,,51,52
SFL,all,PRES,8.5

cmsel,s,sym
DL,all,,symm

!-----------------------Solution
allsel,all
```

```
SBCTRAN
FINISH

/SOL
ANTYPE,0
/STATUS,SOLU
SOLVE
FINISH

/dscale,,3

!-----------------------Reverese Video
/RGB,INDEX,100,100,100, 0
/RGB,INDEX, 80, 80, 80,13
/RGB,INDEX, 60, 60, 60,14
/RGB,INDEX, 0, 0, 0,15
/REPLOT

!-----------------------Post
/POST1
PLNSOL,S,3,2

allsel,all
nsel,s,node,,564
PRNSOL,S,PRIN

allsel,all
lsel,s,line,,3,4
nsll,s,1
PRNSOL,U,Y

!-----------------------Path
allsel,all

!PATH, NAME, nPts, nSets, nDiv

path,1,2,50,40

!PPATH, POINT, NODE, X, Y, Z, CS
path,1
ppath,1,,54/sc,10/sc
ppath,2,,115/sc,10/sc

!Getting the vertical load for the points on path 1

Path,1
PDEF,sy1,S,Y,AVG
/PBC,PATH, ,0
PLPATH,SY1

!Integrating the vertical load over the path to get load bearing shares

PCALC,INTG,int1,SY1,XG,1,
PLPATH,INT1
```